NASA Technical Paper 1876

A Method for Obtaining Reduced-Order Control Laws for High-Order Systems Using Optimization Techniques

Vivek Mukhopadhyay, Jerry R. Newsom,
and Irving Abel

AUGUST 1981

NASA

NASA Technical Paper 1876

A Method for Obtaining Reduced-Order Control Laws for High-Order Systems Using Optimization Techniques

Vivek Mukhopadhyay, Jerry R. Newsom,
and Irving Abel
Langley Research Center
Hampton, Virginia

NASA
National Aeronautics
and Space Administration

**Scientific and Technical
Information Branch**

1981

SUMMARY

A reduced-order control law is synthesized by minimizing a performance index defined by a weighted sum of mean-square steady-state responses and control inputs, as in a stationary linear quadratic Gaussian (LQG) analysis. The order of the control law is assumed to be less than the order of the plant. Gradients of the performance index with respect to the design variables in the reduced-order control law are determined by solving a pair of Lyapunov equations. An analogy with the LQG solution is utilized to select a set of design variables and their initial values. Using the gradients, a nonlinear programming algorithm searches for the control law design variables which minimize the performance index. During the design cycle, an input-noise adjustment procedure is introduced to improve the system's stability margins. Thus an optimal, reduced-order, robust feedback control law can be synthesized without truncating the plant model order.

This control law synthesis method was applied to the synthesis of an active flutter-suppression control law for a wind-tunnel model of an aeroelastic wing represented by a 25th-order plant. The resulting fourth-order control law is shown by analysis to increase the flutter dynamic pressure by at least 44 percent with good stability margins, while minimizing the control input. Although theoretically proven only for a full-order controller, the input-noise adjustment procedure also improved the phase and gain margins for the reduced-order controller. Fourth-order control laws were also obtained by truncation and residualization methods, and results of these control laws were compared with those of the present reoptimization method. The study indicates that by using the present algorithm, nearly optimal low-order control laws with good stability margins can be synthesized.

INTRODUCTION

The state-space equations describing control problems involving flexible structures are usually of high order. This characteristic is particularly true for an aeroelastic system (plant) which requires a large number of states to accurately represent the flexible structure, unsteady aerodynamics, and actuator

dynamics (refs. 1 to 3). The order of a realistic design problem could be 60 or more (refs. 1 and 4). An optimal feedback control law based on the standard linear quadratic Gaussian (LQG) solution would be of the same high order as the plant. This control law (controller) is usually very sensitive to modeling errors, has poor stability margins, and often is too complex to implement in a flight computer. In this paper, a method is developed using optimization techniques for designing a reduced-order control law without these disadvantages.

Reduced-order control laws have been designed using transfer function matching, modal truncation, and residualization techniques (refs. 4 to 6). These methods only approximate the full-order controller, and the resulting control law is no longer optimal. In the present approach, the control law is synthesized by minimizing a performance index defined by a weighted sum of mean-square steady-state responses and control inputs as in a stationary LQG analysis. However, the order of the control law is assumed to be less than the order of the plant. Gradients of the performance index with respect to the design variables of the reduced-order control law are determined by solving a pair of Lyapunov equations. Using the gradients, a nonlinear programing algorithm searches for the design variables which minimize the performance index. The basis of this reduced-order controller design procedure is described in references 7 and 8 and has been applied in reference 9 for attitude control of a flexible spacecraft.

Two problems arise when applying this general method: selection of a set of design variables and their initial values which result in a stable system. In the present paper, a new systematic approach is developed to overcome both problems. The design variables of the reduced-order controller are chosen so that they are analogous to the optimal full-state feedback and Kalman estimator gain matrices. These full-order optimal gain matrices are used for choosing the initial values of the design variables. In the limit when the order of the controller is the same as the order of the plant, the algorithm provides a solution which is identical to the optimal LQG results.

In general, plants using observer-based control laws exhibit poor stability margins. Recently, Doyle and Stein (ref. 10) presented an input-noise adjustment procedure to improve the stability margins of full-order LQG control laws. This procedure is used in the present design algorithm. Results indicate that the procedure can improve the stability margins of the system with a reduced-order control law, although the theoretical proof exists only for a full-order control law.

The method of this paper is then applied to the synthesis of a 4th-order flutter-suppression control law for a wind-tunnel model of an aeroelastic wing, represented by a 25th-order plant. The performance of the flutter-suppression system (FSS) using the reduced-order (4th-order) control law is analyzed and compared with the performance using the corresponding full-order (25th-order) control law. A comparison of results using fourth-order control laws obtained by truncation and residualization methods is also presented.

EQUATIONS OF MOTION IN STATE-SPACE FORM

Plant Model

The equations of motion for an aeroelastic system can be written (refs. 2 and 3) as

$$\left([M]s^2 + [D_s]s + [K]\right)\{\xi_F\} + q\left[\hat{Q}\right]\begin{Bmatrix}\xi_F \\ \xi_C\end{Bmatrix} = q\left[\hat{Q}\right]_G\left\{\frac{\xi_G}{V}\right\} \tag{1}$$

where

$[M]$	generalized mass matrix
$[D_s]$	structural damping matrix
$[K]$	generalized stiffness matrix
s	Laplace variable
ξ_F, ξ_C	generalized coordinate vectors for flexible modes and for control surface deflections
ξ_G	gust velocity vector
q	dynamic pressure
V	free-stream velocity

(The symbols used in this report are listed after the references on page 36.)

The s-plane approximations of the unsteady aerodynamic forces $\left[\hat{Q}\right]$ and $\left[\hat{Q}\right]_G$ are expressed as

$$\left[\hat{Q}\right] = \left[\hat{A}_0\right] + \left[\hat{A}_1\right]\left(\frac{cs}{2V}\right) + \left[\hat{A}_2\right]\left(\frac{cs}{2V}\right)^2 + \sum_{m=1}^{L}\frac{\left[\hat{B}_m\right]s}{\left(s + \frac{2V}{c}\beta_m\right)} \tag{2}$$

where

c	reference chord length

L number of aerodynamic lag terms

β_m aerodynamic lag

The real coefficient matrices $\left[\hat{A}_n\right]$ and $\left[\hat{B}_m\right]$ relate unsteady aerodynamics in the frequency plane to the approximating functions in the s-plane. Unsteady aerodynamic forces on the wing and control surfaces due to sinusoidal motion and gust are generated herein using doublet lattice aerodynamics (ref. 11). By denoting the flexible modes, their time derivatives, and the aerodynamic lag terms within the summation sign in equation (2) by the state variable vector x^*, equation (1) and an accelerometer sensor output equation can be expressed in state-space form (see appendix A) as

$$\{\dot{x}^*\} = [F^*]\{x^*\} + \left[G_1^* \mid G_2^*\right]\{u^*\} \tag{3a}$$

$$\{y\} = \left[H_1^*\right]\{x^*\} + \left[H_2^* \mid H_3^*\right]\{u^*\} \tag{3b}$$

where

F^* dynamics matrix (see eqs. (A7))

G_1^*, G_2^* input matrices (see eqs. (A7))

H_1^*, H_2^*, H_3^* measurement matrices (see eqs. (A9))

and the state vector and input vector are

$$x^* = \left\{\xi_F^T \mid \dot{\xi}_F^T \mid x_{\beta_1}^{*T} \mid x_{\beta_2}^{*T} \mid \cdots \mid x_{\beta_L}^{*T}\right\}^T$$

$$u^* = \left\{\xi_C^T \mid \dot{\xi}_C^T \mid \ddot{\xi}_C^T \mid \xi_G^T \mid \dot{\xi}_G^T \mid \ddot{\xi}_G^T\right\}^T$$

where $x_{\beta_m}^*$ are aerodynamic states (eq. (A3)). As shown in appendix A, the derivative terms in u^* can be eliminated by augmenting x^* with a model of the control surface actuator dynamics and a model of the turbulence. The state-space model of the plant can then be written in the standard form as

$$\dot{x}_s = Fx_s + G_u u + G_w w \tag{4}$$

$$y = Hx_s + v \tag{5}$$

$$y_D = H_D x_s \tag{6}$$

where

x_s augmented plant state vector composed of x^*, actuator states, and turbulence states $(N_S \times 1)$

u control input vector $(N_C \times 1)$

w plant noise vector $(N_W \times 1)$

y measurement output vector $(N_O \times 1)$

v measurement noise vector $(N_O \times 1)$

y_D design output vector $(N_D \times 1)$

and the matrices in equations (4) to (6) are defined in equations (A16), (A17), and (A19). The noise vectors w and v are modeled as zero-mean white noise processes with intensity matrices R_W and R_V, respectively.

Controller Model

A block diagram of the control scheme is shown in figure 1. The controller model is assumed to be

$$\dot{x}_C = Ax_C + By \tag{7}$$

$$u = Cx_C \tag{8}$$

where x_C represents the controller state vector of order M where $M \leq N_S$. The terms A, B, and C are controller dynamics, input, and output matrices of size $M \times M$, $M \times N_O$, and $N_C \times M$, respectively. Of the $M(M + N_O + N_C)$ elements of the A, B, and C matrices, only $M(N_O + N_C)$ are independent (ref. 12) and can be chosen as free design variables. Equation (7) represents a filter which processes the output measurements before being fed back through the gain matrix C. Together, equations (7) and (8) represent a transfer function relation $u = C\left[sI - A\right]^{-1}By$ which is commonly referred to as an output feedback control law.

CONTROL LAW SYNTHESIS METHOD

The control law is synthesized by minimizing a performance index defined by a weighted sum of mean-square steady-state responses and control inputs, as in a stationary LQG analysis. However, the order of the control law is assumed to be less than the order of the plant. Gradients of the performance index with respect to the design variables in the reduced-order control law are determined by solving a pair of Lyapunov equations. An analogy with the LQG solution is

utilized to select a set of design variables and their initial values. Using the gradients, a nonlinear programing algorithm searches for the control law design variables which minimize the performance index. During the design cycle, an input-noise adjustment procedure is introduced to improve the system's stability margins (robustness).

Augmented State Equations

By defining an augmented state vector

$$x_a \equiv \begin{Bmatrix} x_s \\ -- \\ x_c \end{Bmatrix} \tag{9}$$

the closed-loop system is represented by

$$\begin{Bmatrix} \dot{x}_s \\ -- \\ \dot{x}_c \end{Bmatrix} = \left[\begin{array}{c:c} F & G_u C \\ \hline BH & A \end{array}\right] \begin{Bmatrix} x_s \\ -- \\ x_c \end{Bmatrix} + \left[\begin{array}{c:c} G_w & 0 \\ \hline 0 & B \end{array}\right] \begin{Bmatrix} w \\ \hline v \end{Bmatrix} \tag{10}$$

or

$$\dot{x}_a \equiv F_a x_a + G_a \eta$$

If F_a is stable with the chosen values of A, B, and C, the covariance of x_a reaches a steady-state value which satisfies the Lyapunov equation given by

$$F_a X_a + X_a F_a^T = -G_a R_a G_a^T \tag{11}$$

where

$$X_a \equiv \lim_{t\to\infty} E\left[x_a x_a^T\right] \equiv \left[\begin{array}{c:c} X_s & X_{sc} \\ \hline X_{sc}^T & X_c \end{array}\right] \tag{12}$$

and

$$R_a \equiv \left[\begin{array}{c:c} R_w & 0 \\ \hline 0 & R_v \end{array}\right] \tag{13}$$

Performance Index

The control law is synthesized using a conjugate gradient algorithm (ref. 13) to search for the $M(N_o + N_c)$ design variables of the Mth-order control law (eqs. (7) and (8)) which minimize a performance index J defined by

$$J = \lim_{t\to\infty} E\left[y_D{}^T Q_1 y_D + u^T Q_2 u\right]$$

$$= \mathrm{tr}\left[\left(H_D{}^T Q_1 H_D\right) X_s\right] + \mathrm{tr}\left[Q_2 U\right] \tag{14}$$

where Q_1 and Q_2 are symmetric weighting matrices and X_s and U are steady-state covariance matrices of the states x_s and control inputs u, respectively. Substituting equation (8) into equation (14) and using the definitions given by equations (9) and (12) result in

$$J = \mathrm{tr}\left[\left[\begin{array}{c|c} H_D{}^T Q_1 H_D & 0 \\ \hline 0 & C^T Q_2 C \end{array}\right]\left[\begin{array}{c|c} X_s & X_{sc} \\ \hline X_{sc}{}^T & X_c \end{array}\right]\right] \equiv \mathrm{tr}\left[Q_a X_a\right] \tag{15}$$

Gradients

It is shown in appendix B that the gradients of J with respect to the elements of the matrices A, B, and C can be expressed as

$$\frac{\partial J}{\partial A} = 2\left[\Lambda_{sc}{}^T X_{sc} + \Lambda_c X_c\right] \tag{16}$$

$$\frac{\partial J}{\partial B} = 2\left[\left(\Lambda_{sc}{}^T X_s + \Lambda_c X_{sc}{}^T\right) H^T + \Lambda_c B R_v\right] \tag{17}$$

$$\frac{\partial J}{\partial C} = 2\left[Q_2 C X_c + G_u{}^T\left(\Lambda_s X_{sc} + \Lambda_{sc} X_c\right)\right] \tag{18}$$

where Λ is a $(N_s + M) \times (N_s + M)$ symmetric Lagrange multiplier matrix defined as

$$\Lambda \equiv \left[\begin{array}{c|c} \Lambda_s & \Lambda_{sc} \\ \hline \Lambda_{sc}^T & \Lambda_c \end{array}\right] \tag{19}$$

which satisfies the dual Lyapunov equation

$$F_a^T \Lambda + \Lambda F_a = -Q_a \tag{20}$$

Design Variables

There are several possible ways of selecting a set of $M(N_o + N_c)$ free design variables of the control law (eqs. (7) and (8)). In a canonical form of the control law, the coefficients of numerator and common denominator polynomials can be identified as the design variable set. In a block diagonal form, the real and imaginary parts of the controller poles and numerator residues can be taken as the design variable set. While these representations can be incorporated into the present algorithm (to optimize an existing control law in transfer function form), they are not very general and are often inconvenient from a matrix bookkeeping point of view. Also the initial values of the design variables can be difficult to estimate. In the present method the $M(N_o + N_c)$ elements of B and C are chosen as the free design variables and a subset of the Kalman estimator gain and optimal full-state feedback gain matrices obtained from the LQG solution are chosen as their initial values. The justification is as follows.

If for a full-order controller ($M = N_s$), we let $A = F - BH + G_u C$ and use the elements of B and C as design variables, then it is shown in appendix C that the optimized values of B and C are identical to the steady-state Kalman estimator gain and optimal full-state feedback gain matrices, respectively. The controller states x_c are identified as the asymptotic estimates of the plant states x_s. By analogy, when $M < N_s$, the low-order controller may be treated as a partial estimator of M key states denoted by $x_1 \equiv Rx_s$ (R is a Boolian matrix of order $M \times N_s$). A full discussion of this approach and the asymptotic behavior of the estimation error is presented in appendix D.

Thus we initially set

$$A = R(F - B_o H + G_u C_o) R^T \tag{21}$$

$$B = RB_o \tag{22}$$

$$C = C_o R^T \tag{23}$$

where M key states are chosen for estimation. The matrices B_o and C_o are the full-order Kalman estimator and optimal full-state feedback gain matrices, respectively. Subsequently,

$$A = RFR^T - BHR^T + RG_uC \tag{24}$$

Since A is a function of B and C, the total gradients of J with respect to B and C are given by

$$\left.\begin{aligned} \frac{dJ}{dB} &= \frac{\partial J}{\partial B} - \frac{\partial J}{\partial A} RH^T \\ \frac{dJ}{dC} &= \frac{\partial J}{\partial C} + \left[RG_u\right]^T \frac{\partial J}{\partial A} \end{aligned}\right\} \tag{25}$$

Substituting the partial gradients from equations (16) to (18) in equations (25) results in

$$\left.\begin{aligned} \frac{dJ}{dB} &= 2\left[\left(\Lambda_{sc}{}^T X_s + \Lambda_c X_{sc}{}^T\right)H^T - \left(\Lambda_{sc}{}^T X_{sc} + \Lambda_c X_c\right)RH^T + \Lambda_c BR_v\right] \\ \frac{dJ}{dC} &= 2\left[Q_2 C X_c + G_u{}^T\left(\Lambda_s X_{sc} + \Lambda_{sc} X_c\right) + \left(RG_u\right)^T\left(\Lambda_{sc}{}^T X_{sc} + \Lambda_c X_c\right)\right] \end{aligned}\right\} \tag{26}$$

With the performance index J and its gradients known, a conjugate gradient optimization procedure (ref. 13) can be used to minimize J. The $(N_s + M)$th order Lyapunov equations are solved by a program described in reference 14. This process is feasible only if F_a is a stable matrix for each iteration.

Robustness Recovery Technique

Plants using full-order LQG controllers usually exhibit poor stability margins. It has been shown in reference 10 that by introducing a fictitious input noise η_u of intensity R_u in equation (8) (the noise is not included in the performance index directly) and by increasing R_u by a scalar factor, the full-order controller system loop transfer function (loop broken at u) asymptotically approaches the corresponding full-state feedback loop transfer function (and hence they have the same stability properties). This input-noise adjustment procedure is incorporated in the present reduced-order controller design process by replacing G_w and w in equation (10) by $\left[G_u \mid G_w\right]$ and $\left[\eta_u{}^T \mid w^T\right]^T$, respectively. Consequently, R_w in equation (13) is replaced by

$$\left[\begin{array}{c|c} R_u & 0 \\ \hline 0 & R_w \end{array}\right]$$

The resulting effect is an additional noise term $G_u R_u G_u^T$ in the first $N_s \times N_s$ sets of Lyapunov equation (11). In appendix D, it is shown that η_u appears as an additional noise parameter in the partial state estimation error dynamics. Although not proven theoretically, numerical results show that this input-noise adjustment procedure is also capable of improving stability margins of the plant with a reduced-order controller. The input-noise intensity matrix R_u becomes a major design parameter in this controller synthesis technique.

Design Algorithm

A block diagram of the design algorithm is shown in figure 2. The design algorithm consists of the following steps:

1. Obtain B_o and C_o.
2. Select M key states (matrix R).
3. Compute RFR^T, RG_u, HR^T, $B = RB_o$, and $C = C_o R^T$.
4. Set $A = RFR^T - BHR^T + RG_uC$.
5. Test F_a for stability.
6. If F_a is stable, solve Lyapunov equations (11) and (20) for X_a and Λ.
7. Compute J, dJ/dB, and dJ/dC.
8. Obtain the next set of B and C by a conjugate gradient algorithm.
9. Repeat steps 4 through 8 with new values of B and C until J converges to a minimum value.

In step 2, it is often convenient to transform the plant state equations to a block diagonal form for easier selection of key states to be estimated. If F_a is initially unstable in step 5, then either select a new set of states or select a new value of R_u and return to step 1, until a stable F_a is obtained. If F_a becomes unstable during a linear search in the optimization process, the algorithm automatically searches in a new direction from the last stable F_a solution.

APPLICATION TO FLUTTER SUPPRESSION

Model Description

The control law synthesis method described in the previous sections is applied to the synthesis of an active flutter-suppression control law for an

aeroelastic wind-tunnel model. The geometry of the cantilever wing model, along with the control surface and sensor (accelerometer) locations, is shown in figure 3. The model is described in detail in reference 1. The state-space equations are derived using five flexible modes and two aerodynamic lag terms ($L = 2$, $\beta_1 = 0.225$, $\beta_2 = 0.5$). All structural damping is assumed to be zero. The actuator dynamics are represented by a third-order transfer function given by (ref. 1):

$$\frac{\xi_C}{\delta_C} = \frac{(214)(89\ 450)}{(s + 214)(s^2 + 179.45s + 89\ 450)} \frac{\text{deg}}{\text{deg}} \tag{27}$$

A turbulence model represented by the following second-order transfer function is used to approximate a Dryden gust spectrum:

$$\frac{\xi_G}{w} = \frac{\sigma_{wg}\sqrt{\frac{3V}{\ell}}\left(s + \frac{V}{\ell\sqrt{3}}\right)}{\left(s + \frac{V}{\ell}\right)^2} (\text{m/sec})\sqrt{\text{sec}} \tag{28}$$

where

σ_{wg} root-mean-square (rms) gust velocity, m/sec

ℓ scale of turbulence or characteristic length, m

V flight velocity, m/sec

For numerical calculation $\ell = 30.48$ m and $\sigma_{wg} = 1$. The resulting plant model is a single-input single-output system of order 25. The input u is the actuator command signal δ_C and the output y is the accelerometer signal $\ddot{z}$. The dynamic-pressure root locus at Mach 0.9 is shown in figure 4 without the flutter-suppression system. Flutter is predicted at a dynamic pressure of 4.7 kPa and a frequency of 50 rad/sec. The present objective is to design a low-order control law which will increase the maximum operating dynamic pressure by 44 percent above the experimental flutter dynamic pressure of 5.32 kPa (ref. 1), with minimum control surface activity and adequate stability margins. The control law design point is thus chosen to be a dynamic pressure of 7.66 kPa at Mach 0.9.

Control Laws

Full-order control law.- For comparison purposes, the full-order control law, which is identical to the LQG solution, is obtained first. The design output matrix H_D is chosen to be the same as the sensor output matrix H. The weighting matrices, which are scalars for this single-input single-output system, are selected to be $Q_1 = 0.0001$, $Q_2 = 50\ 000$, $R_w = 1.0$, and $R_v = 1.0$.

This choice of weighting nearly reflects the unstable pole about the imaginary axis without affecting the stable poles. The unit plant noise intensity matrix R_w results in unit rms gust velocity in equation (28). The control laws are designed at three values of R_u, namely 0, 0.00001, and 0.0001. Numerical values of all these parameters were chosen on the basis of some preliminary results obtained with a 20th-order plant model (ref. 15). To determine the improvements in the control law designed with increasing R_u, the phase and gain margins of the plant plus the control law are determined. The Nyquist diagrams of the plant with the full-order output feedback control law, presented in figure 5, show a progressive increase in phase and gain margins. As predicted in reference 10, the Nyquist diagram asymptotically approaches the full-state feedback result which is a circle of unit radius centered at (-1,0). The price paid is an increase in the optimal design performance index J and associated increases in rms values of the input and output (table I). The closed-loop dynamic-pressure root locus using the full-order control law designed with $R_u = 0.00001$ is presented in figure 6. The flutter dynamic pressure is increased to 9.0 kPa. Beyond this point, the control law complex pole (filter mode) is unstable.

Fourth-order control law.- Fourth-order control laws were synthesized by selecting the first two flexible modes and their time derivatives as the four key states. The initial values of the gain matrices B and C were obtained from the full-order results. In transfer function form, the control laws designed with the three values of R_u are, respectively

$$\frac{u}{\ddot{z}} = \frac{(-364.4)(s - 136.4)(s^2 + 73.69s + 5697)}{(s + 2.057)(s + 2057)(s^2 + 46.37s + 2047)} \text{ deg/g unit} \qquad (R_u = 0) \qquad (29)$$

$$\frac{u}{\ddot{z}} = \frac{(1939.4)(s + 24.74)(s^2 + 87.63s + 13\ 806)}{(s + 3.864)(s + 3270)(s^2 + 20.97s + 1423)} \text{ deg/g unit} \quad (R_u = 0.00001) \qquad (30)$$

$$\frac{u}{\ddot{z}} = \frac{(1424.6)(s + 31.90)(s^2 + 100.0s + 12\ 210)}{(s + 1.798)(s + 2541)(s^2 + 17.76s + 1547)} \text{ deg/g unit} \quad (R_u = 0.0001) \qquad (31)$$

Figure 7 shows a typical convergence pattern of the performance index obtained in the course of synthesizing control law (eq. (30)). Convergence is assumed when the change in the performance index is less than 0.1 percent of its initial value for three successive iterations. Most of the reduction in the performance index is achieved in the first few iterations. The optimized performance index is within 16 percent of the full-order controller performance index.

The Nyquist diagrams of the plant plus fourth-order controllers given by equations (29) to (31) are presented in figure 8. With the control law designed without input noise (eq. (29)), the stability margins are poor and relatively unaffected by controller order reduction. Although theoretically proven only

for a full-order controller, it is interesting to note that the input-noise adjustment procedure of reference 10 is also capable of improving the phase and gain margins for a reduced-order controller. For a given R_u, reducing the controller from full order to fourth order results in only a slight degradation (increase) in the optimal design performance index J (table I).

As a compromise between better stability margins and lower control surface motion (deflection and deflection rate), the controller given by equation (30), i.e., designed with $R_u = 0.00001$, was selected for overall performance analysis and comparison. The dynamic-pressure root locus using the fourth-order optimal control law of equation (30) is shown in figure 9. The closed-loop flutter dynamic pressure is 8.7 kPa. Beyond this point, the controller complex pole (filter mode) is unstable. A Bode plot of the plant plus this control law is presented in figure 10 and compared with the corresponding plot for the full-order case. The plots compare quite well up to approximately 400 rad/sec. A sharp drop in amplitude at 400 rad/sec for the fourth-order case is due to a zero in the plant ($\ddot{z}/\delta_c$) transfer function. For the full-order case, this sharp drop in amplitude is removed by cancellation of the plant zero by a controller pole.

The lowest order of the controller obtained in the course of this study is four. Higher order controllers are possible but do not result in substantial performance improvement.

CONTROL LAW PERFORMANCE

In this section, the performance of the fourth-order controller designed with $R_u = 0.00001$ (eq. (30)) is discussed and compared with the corresponding full-order (LQG) controller.

Flutter Characteristics

The dynamic-pressure root locus diagrams of the plant with the full 25th-order controller and 4th-order controller (eq. (30)) are presented in figures 6 and 9, respectively. The first two modes and the controller complex pole (filter mode) are less damped for the fourth-order controller than for the full-order controller, at dynamic pressures of 7.66 kPa and lower. The higher modes remain relatively unaffected by both control laws. With the full-order controller, the flutter dynamic pressure is increased by 91 percent (from 4.7 kPa to 9.0 kPa), whereas with the fourth-order controller, the increase is 85 percent (to 8.7 kPa). Thus, the flutter-suppression performance deterioration due to this reduction in controller order is only 6 percent. In both cases, beyond the flutter point, the controller complex pole is unstable at a frequency of 40 rad/sec.

Stability Margins

To examine the stability margins of the plant plus the control laws at off-design dynamic pressures, the phase and gain margins of this single-input

single-output system were computed over a range of dynamic pressures up to the design value (7.66 kPa) and are presented in figure 11. With the fourth-order controller at the design dynamic pressure, the gain margins are -5 dB and +12.3 dB. The phase margins are -46° and $+53^{\circ}$. The closed-loop system is stable over the entire range of dynamic pressures, and a ±5 dB gain margin and $\pm 30^{\circ}$ phase margin are maintained over the dynamic-pressure range from 5.7 kPa to 7.66 kPa. This provides a measure of insensitivity of the designed active-control system to dynamic-pressure variation. Except for the positive phase margins which fall below $+30^{\circ}$ at dynamic pressures of 5.7 kPa and lower (fig. 11), all the other margins improve with decreasing dynamic pressure. Since the stability margins with the full-order controller also exhibit almost the same characteristics (shown by dashed line in fig. 11), the deterioration in positive phase margin is not due to the controller order reduction.

Steady-State Response

Table I presents the steady-state root-mean-square (rms) responses of the control input u_{rms}, control surface deflection δ_{rms}, deflection rate $\dot{\delta}_{rms}$, and sensor output $\ddot{z}_{rms}$ at the design dynamic pressure using the fourth-order controllers (eqs. (29) to (31)) and corresponding full-order controllers. These values were obtained by setting $R_u = 0$ and executing the usual covariance analysis with the optimized control law. With the fourth-order controller designed with $R_u = 0.00001$ (eq. (30)), δ_{rms} and $\dot{\delta}_{rms}$ are 17.0° and 756.0 deg/sec, respectively (all calculations performed for a 1 m/sec rms gust velocity). The respective values with the corresponding full-order controller are slightly higher. These values are in the vicinity of the typical maximum allowable limits.

To examine the steady-state δ_{rms}, $\dot{\delta}_{rms}$, and $\ddot{z}_{rms}$ at off-design dynamic pressures, their values normalized by their design-point values are presented in figure 12 for the fourth-order controller designed with $R_u = 0.00001$ (eq. (30)). These responses are computed with $R_u = 0$ and $R_v = 0$ and are slightly lower than those with $R_v = 1.0$. Figure 12 indicates that for dynamic pressures below the design point, δ_{rms}, $\dot{\delta}_{rms}$, and $\ddot{z}_{rms}$ are consistently lower than their design-point values except for $\ddot{z}_{rms}$ at 6.7 kPa which is 2.6 percent higher. The deterioration of positive phase margin at lower dynamic pressures (fig. 11) does not adversely affect the system steady-state response.

Transient Response

The present design technique is based on minimizing the system input and output at steady state. Therefore, it is important to check the transient response with the designed controllers. The state transition matrix technique (ref. 14) was used to determine δ, $\dot{\delta}$, and $\ddot{z}$ responses to a 1° step pulse of

0.01-second duration as an input command for the full- and fourth-order controllers at the design dynamic pressure. These responses are shown in figure 13.

The responses using the fourth-order controller are quite similar to those using the full-order controller and decay rapidly in a few cycles. The peak values are $\delta = 1^{o}$, $\dot{\delta} = -200$ deg/sec, and $\ddot{z} = 0.6g$, respectively. These are somewhat higher than values for the full-order controller. The lower damping of the plant with the fourth-order controller is consistent with the earlier observation from the root-locus diagrams (figs. 6 and 9).

Performance With 65th-Order Plant Model

The 4th-order controller of equation (30) was designed using a 25th-order state-space model of the plant obtained using five flexible modes and two aerodynamic lag terms. In order to examine the performance of this control law with a more accurate state-space model of the plant, it was applied to a 65th-order plant model obtained by including the first 10 flexible modes and 4 aerodynamic lag terms ($L = 4$, $\beta_1 = 0.2$, $\beta_2 = 0.4$, $\beta_3 = 0.6$, $\beta_4 = 0.8$). The actuator dynamics and turbulence models (eqs. (27) and (28)) remained the same. The Nyquist diagram of this 65th-order plant plus the 4th-order controller of equation (30) at the design dynamic pressure is presented in figure 14. The gain margins are -5.4 dB at 62 rad/sec and +12.0 dB at 310 rad/sec. The phase margins are -62^{o} at 45 rad/sec and $+57^{o}$ at 82 rad/sec. These margins are slightly better than those with the 25th-order plant model (fig. 8(b)). The stability margins at lower dynamic pressures (not presented) are similar to those of figure 11. The dynamic-pressure root locus of the 65th-order plant plus the 4th-order controller is presented in figure 15. All the modes not included in the original 25th-order plant used for the controller design are found to be stable. The flutter dynamic pressure is 8.85 kPa. Beyond this point, the controller complex pole (filter mode) is unstable at a frequency of 40 rad/sec.

COMPARISON WITH TRUNCATED AND RESIDUALIZED CONTROL LAWS

Reduced-order control laws can also be obtained from optimal control theory results by truncation and residualization methods. In the truncation method, the low-order controller is obtained by partitioning the optimal full-state feedback and Kalman estimator gain matrices and retaining only the part of the optimal controller corresponding to the key states and their first derivatives. In the residualization method (ref. 6), a first-order correction is added by retaining the static part of the controller corresponding to the rest of the states. The present method can be considered a reoptimization of the truncated control law. For a comparison of the performance of the control laws obtained by these three related methods, 4th-order control laws are also designed by truncation and residualization methods using identical base data and noise intensities ($R_u = 0.00001$) for the 25th-order plant at the design dynamic pressure. The Nyquist diagrams of the plant plus the full-order controller and of the plant plus 4th-order truncated, residualized, and reoptimized control laws are presented in figure 16. The corresponding stability margins are presented in table II. For the truncation method, the gain margins are -10.3 dB and

+6.5 dB, and the phase margins are -17° and $+57^{\circ}$. For the residualization method, the gain margins are -7.1 dB and +6.0 dB, and the phase margins are -55° and $+38^{\circ}$. The shapes of the corresponding Nyquist diagrams (figs. 16(b) and (c)) indicate that the phase and positive gain margins would decrease rapidly with increase in gain. In comparison, for the present method, the overall stability margins are better and closer to the full-order optimal result. Since the corresponding Nyquist diagram is nearly circular around (-1,0) (fig. 16(d)), the stability margins are less sensitive to change in gain.

The root-mean-square (rms) values of the steady-state responses δ_{rms}, $\dot{\delta}_{rms}$, and $\ddot{z}_{rms}$ using the control laws designed by the three methods are presented in table II along with the corresponding values using the full-order optimal LQG controller, for comparison. These values are computed using $R_u = 0$ and correspond to the steady-state response due to a 1 m/sec rms gust. The present method yields the lowest δ_{rms}, while the lowest $\dot{\delta}_{rms}$ is obtained by the residualization method. The truncation method provides the lowest $\ddot{z}_{rms}$. In general, except in the truncation method, the control surface rms responses are of the same order.

CONCLUSIONS

A method of synthesizing reduced-order optimal feedback control laws for a high-order system is developed. A design algorithm which employs a nonlinear programing technique and an analogy with the LQG solution is presented. An input-noise adjustment procedure is used to improve the stability margins of the system. This general method is applied to the synthesis of an active flutter-suppression control law for a wind-tunnel model of an aeroelastic wing. The important results of this study are the following:

1. The present method can be used to synthesize optimal, reduced-order, robust feedback control laws for a high-order plant without truncating the plant model order. It is applicable to a multi-input, multi-output system.

2. Application of this method to a 25th-order plant representing an aeroelastic wing model provides a 4th-order flutter-suppression control law which is shown by analysis to increase the flutter dynamic pressure by at least 44 percent (at Mach of 0.9) with good stability margins while minimizing the control input.

3. The numerical results indicate that the input-noise adjustment procedure of Doyle and Stein is capable of improving the stability margins of the system with a reduced-order controller, although the theoretical proof exists only for a full-order controller.

4. The present reoptimization algorithm appears to provide better control laws than those obtained by truncation and residualization methods.

Langley Research Center
National Aeronautics and Space Administration
Hampton, VA 23665
June 17, 1981

APPENDIX A

STATE-SPACE EQUATIONS

The detailed derivation of equations (3) to (6) are presented in this appendix.

Plant Equation

Let us define the vectors

$$\left\{x^*_{F_1}\right\} \equiv \left\{\xi_F\right\} \tag{A1}$$

$$\left\{x^*_{F_2}\right\} \equiv s\left\{\xi_F\right\} \tag{A2}$$

$$\left\{x^*_{\beta_m}\right\} \equiv \frac{q\left[\hat{B}_m\right]}{\left(s + \frac{2V}{c}\,\beta_m\right)}\begin{Bmatrix} s\xi_F \\ s\xi_C \end{Bmatrix} - \frac{q\left[\hat{B}_m\right]_G}{\left(s + \frac{2V}{c}\,\beta_m\right)}\begin{Bmatrix} s\xi_G \\ \overline{V} \end{Bmatrix} \qquad (m = 1, 2, \ldots, L) \tag{A3}$$

and also define the following matrices

$$\left.\begin{aligned} \left[\tilde{M}\right] &\equiv \left[M\right] + q\left(\frac{c}{2V}\right)^2\left[\hat{A}_2\right]_F \\ \left[\tilde{D}\right] &\equiv \left[D_s\right] + q\left(\frac{c}{2V}\right)\left[\hat{A}_1\right]_F \\ \left[\tilde{K}\right] &\equiv \left[K\right] + q\left[\hat{A}_0\right]_F \end{aligned}\right\} \tag{A4}$$

Separate the control surface and flexible mode components by partitioning the the matrices $\left[\hat{A}_n\right]$ and $\left[\hat{B}_m\right]$ as

$$\left[\hat{A}_n\right] = \left[\left[\hat{A}_n\right]_F \;\vdots\; \left[\hat{A}_n\right]_C\right] \qquad (n = 0, 1, 2) \tag{A5}$$

$$\left[\hat{B}_m\right] = \left[\left[\hat{B}_m\right]_F \;\vdots\; \left[\hat{B}_m\right]_C\right] \qquad (m = 1, 2, \ldots, L) \qquad \text{(A6)}$$

Then by using the definitions in equations (A1) to (A6), equation (1) can be written as shown in matrix equation (A7a) on page 21. With zero initial conditions assumed, equation (A7a) is denoted by equation (3a) in the time domain:

$$\left\{\dot{x}^*\right\} = \left[F^*\right]\left\{x^*\right\} + \left[G_1^* \;\vdots\; G_2^*\right]\left\{u^*\right\} \qquad \text{(A7b)}$$

Sensor Output Equation

An accelerometer sensor output equation can be expressed as

$$\left\{y\right\} = \left[\Phi\right]\left\{\ddot{\xi}_F\right\} \qquad \text{(A8)}$$

where $\left[\Phi\right]$ is a matrix of modal amplitudes at the sensor location. Using the definition in equation (A2) and the second row of equation (A7a), equation (A8) can be written as

$$\left\{y\right\} = \left[\Phi\right]\left\{\dot{x}_{F_2}^*\right\} = -\left[\Phi\right]\left[\tilde{M}\right]^{-1}\left[\left[\tilde{K}\right] \;\vdots\; \left[\tilde{D}\right] \;\vdots\; [I] \;\vdots\; [I] \;\vdots\; \cdots \;\vdots\; [I]\right]\begin{Bmatrix} x_{F_1}^* \\ x_{F_2}^* \\ x_{\beta_1}^* \\ x_{\beta_2}^* \\ \vdots \\ x_{\beta_L}^* \end{Bmatrix}$$

$$+ q\left[\Phi\right]\left[\tilde{M}\right]^{-1}\left[-\left[\hat{A}_0\right]_C \;\vdots\; -\left[\hat{A}_1\right]_C\left(\frac{c}{2V}\right) \;\vdots\; -\left[\hat{A}_2\right]_C\left(\frac{c}{2V}\right)^2 \;\Big|\; \left[\hat{A}_0\right]_G \;\vdots\; \left[\hat{A}_1\right]_G\left(\frac{c}{2V}\right) \;\vdots\; \left[\hat{A}_2\right]_G\left(\frac{c}{2V}\right)^2\right]\begin{Bmatrix} \xi_C \\ \dot{\xi}_C \\ \ddot{\xi}_C \\ \hline \xi_G \\ \dot{\xi}_G \\ \ddot{\xi}_G \end{Bmatrix} \qquad \text{(A9a)}$$

$$
s\begin{Bmatrix} x^*_{F_1} \\ x^*_{F_2} \\ x^*_{\beta_1} \\ x^*_{\beta_2} \\ \vdots \\ x^*_{\beta_L} \end{Bmatrix} = \begin{bmatrix} 0 & [I] & 0 & 0 & \cdots & 0 \\ -[\tilde{M}]^{-1}[\tilde{K}] & -[\tilde{M}]^{-1}[\tilde{D}] & -[\tilde{M}]^{-1} & -[\tilde{M}]^{-1} & \cdots & -[\tilde{M}]^{-1} \\ 0 & q\left[\hat{B}_1\right]_F & -\frac{2V}{c}\beta_1 & 0 & \cdots & 0 \\ 0 & q\left[\hat{B}_2\right]_F & 0 & -\frac{2V}{c}\beta_2 & \cdots & 0 \\ \vdots & \vdots & \vdots & \vdots & \cdots & \vdots \\ 0 & q\left[\hat{B}_L\right]_F & 0 & 0 & \cdots & -\frac{2V}{c}\beta_L \end{bmatrix} \begin{Bmatrix} x^*_{F_1} \\ x^*_{F_2} \\ x^*_{\beta_1} \\ x^*_{\beta_2} \\ \vdots \\ x^*_{\beta_L} \end{Bmatrix}
$$

$$
+ q \left[\begin{array}{ccc:ccc} 0 & 0 & 0 & 0 & 0 & 0 \\ -[\tilde{M}]^{-1}\left[\hat{A}_0\right]_C & -[\tilde{M}]^{-1}\left[\hat{A}_1\right]_C\left(\frac{c}{2V}\right) & -[\tilde{M}]^{-1}\left[\hat{A}_2\right]_C\left(\frac{c}{2V}\right)^2 & [\tilde{M}]^{-1}\left[\hat{A}_0\right]_G & [\tilde{M}]^{-1}\left[\hat{A}_1\right]_G\left(\frac{c}{2V}\right) & [\tilde{M}]^{-1}\left[\hat{A}_2\right]_G\left(\frac{c}{2V}\right)^2 \\ 0 & \left[\hat{B}_1\right]_C & 0 & 0 & -\left[\hat{B}_1\right]_G & 0 \\ 0 & \left[\hat{B}_2\right]_C & 0 & 0 & -\left[\hat{B}_2\right]_G & 0 \\ \vdots & \vdots & \vdots & \vdots & \vdots & \vdots \\ 0 & \left[\hat{B}_L\right]_C & 0 & 0 & -\left[\hat{B}_L\right]_G & 0 \end{array}\right] \begin{Bmatrix} \xi_C \\ s\xi_C \\ s^2\xi_C \\ \hline \xi_G \\ s\xi_G \\ s^2\xi_G \end{Bmatrix}
$$

Matrix equation (A7a)

or

$$\{y\} \equiv \left[H_1^*\right]\left\{x^*\right\} + \left[H_2^* \mid H_3^*\right]\{u^*\} \tag{A9b}$$

Thus, equation (3b) is obtained.

Actuator and Turbulence State Equations

The actuator transfer function can be expressed in state-space form as

$$\left.\begin{aligned} \left\{\dot{x}_{ac}^*\right\} &= \left[A_{ac}^*\right]\left\{x_{ac}^*\right\} + \left[B_{ac}^*\right]\{u\} \\ \begin{Bmatrix} \xi_C \\ \dot{\xi}_C \\ \ddot{\xi}_C \end{Bmatrix} &= \left[C_{ac}^*\right]\left\{x_{ac}^*\right\} \end{aligned}\right\} \tag{A10}$$

where A_{ac}^*, B_{ac}^*, and C_{ac}^* are the dynamics matrix, the control distribution matrix, and the output matrix of the actuator and $\{u\}$ is the actuator command input. The order of the actuator state vector is the order of the denominator in the actuator transfer function. A model of the turbulence is used whose power spectral density approximates the power spectral density of the gust velocity. The model of the turbulence can be expressed as a Markov's process

$$\left.\begin{aligned} \left\{\dot{x}_G^*\right\} &= \left[A_G^*\right]\left\{x_G^*\right\} + \left[B_G^*\right]\{w\} \\ \begin{Bmatrix} \xi_G \\ \dot{\xi}_G \\ \ddot{\xi}_G \end{Bmatrix} &= \left[C_G^*\right]\left\{x_G^*\right\} \end{aligned}\right\} \tag{A11}$$

where A_G^*, B_G^*, and C_G^* are the dynamics, control distribution, and output matrices of the turbulence and $\{w\}$ is a white noise process.

APPENDIX A

Plant State Equation

Equations (A10) and (A11) can be combined and written as

$$\{u^*\} = \begin{bmatrix} C^*_{ac} & \vdots & 0 \\ \cdots & \vdots & \cdots \\ 0 & \vdots & C^*_G \end{bmatrix} \begin{Bmatrix} x^*_{ac} \\ x^*_G \end{Bmatrix} \tag{A12}$$

$$\begin{Bmatrix} \dot{x}^*_{ac} \\ \dot{x}^*_G \end{Bmatrix} = \begin{bmatrix} A^*_{ac} & \vdots & 0 \\ \cdots & \vdots & \cdots \\ 0 & \vdots & A^*_G \end{bmatrix} \begin{Bmatrix} x^*_{ac} \\ x^*_G \end{Bmatrix} + \begin{bmatrix} B^*_{ac} & \vdots & 0 \\ \cdots & \vdots & \cdots \\ 0 & \vdots & B^*_G \end{bmatrix} \begin{Bmatrix} u \\ w \end{Bmatrix} \tag{A13}$$

By augmenting the vector $\{x^*\}$ with $\begin{Bmatrix} x^*_{ac} \\ x^*_G \end{Bmatrix}$ and substituting equation (A12) into equation (A7b), equations (3a) and (A13) can be written as

$$\begin{Bmatrix} \dot{x}^* \\ \dot{x}^*_{ac} \\ \dot{x}^*_G \end{Bmatrix} = \begin{bmatrix} F^* & \vdots & G^*C^*_{1ac} & \vdots & G^*C^*_{2G} \\ \cdots & \vdots & A^*_{ac} & \vdots & \cdots \\ 0 & \vdots & \cdots & \vdots & A^*_G \end{bmatrix} \begin{Bmatrix} x^* \\ x^*_{ac} \\ x^*_G \end{Bmatrix} + \begin{bmatrix} 0 & \vdots & 0 \\ \cdots & \vdots & \cdots \\ B^*_{ac} & \vdots & 0 \\ \cdots & \vdots & \cdots \\ 0 & \vdots & B^*_G \end{bmatrix} \begin{Bmatrix} u \\ w \end{Bmatrix} \tag{A14}$$

By defining

$$x_s \equiv \begin{Bmatrix} x^* \\ x^*_{ac} \\ x^*_G \end{Bmatrix} \tag{A15}$$

$$F \equiv \begin{bmatrix} F^* & \vdots & G^*C^*_{1ac} & \vdots & G^*C^*_{2G} \\ \cdots & \vdots & A^*_{ac} & \vdots & \cdots \\ 0 & \vdots & \cdots & \vdots & A^*_G \end{bmatrix} \tag{A16}$$

$$G_u \equiv \begin{bmatrix} 0 \\ \hline B^*_{ac} \\ \hline 0 \end{bmatrix} \qquad G_w \equiv \begin{bmatrix} 0 \\ \hline 0 \\ \hline B^*_G \end{bmatrix} \tag{A17}$$

one can denote equation (A14) by equation (4).

Sensor Output Equation in State Variables

Substituting equation (A12) into equation (A9b), one obtains

$$\{y\} = \left[H^*_1 \mid H^*_2 C^*_{ac} \mid H^*_3 C^*_G\right] \begin{Bmatrix} x^* \\ x^*_{ac} \\ x^*_G \end{Bmatrix} + \{v\} \tag{A18}$$

where a white noise process $\{v\}$ is added to represent measurement uncertainties.

Defining

$$H \equiv \left[H^*_1 \mid H^*_2 C^*_{ac} \mid H^*_3 C^*_G\right] \tag{A19}$$

and using the definition of the state vector $\{x_s\}$ in equation (A15) results in equation (5). In a similar manner any design output vector $\{y_D\}$ can be written in terms of $\{x_s\}$ to obtain equation (6).

APPENDIX B

GRADIENT OF PERFORMANCE INDEX

Minimization of the performance index J defined by equation (15) in which the covariance matrix X_a satisfies the Lyapunov equation (11) can be treated as a constrained optimization problem. Equation (15) can be written as

$$J = \mathrm{tr}\left[Q_a X_a + \Lambda^T\left(F_a X_a + X_a F_a^T + G_a R_a G_a^T\right)\right] \tag{B1}$$

where Λ is a Lagrange multiplier matrix. Define a matrix $\hat{P}$ as

$$\hat{P} \equiv \left[\begin{array}{c|c} 0 & C \\ \hline B & A \end{array}\right]_{(N_C+M)\times(N_O+M)} \tag{B2}$$

The necessary conditions for minimization of equation (B1) with respect to $\hat{P}$ are then equation (11) (from $\partial J/\partial\Lambda = 0$) along with

$$0 = \frac{\partial J}{\partial X_a} = \left[Q_a^T + F_a^T\Lambda + \Lambda F_a\right] \tag{B3}$$

$$0 = \frac{\partial J}{\partial \hat{P}_{ij}} = \mathrm{tr}\left[\frac{\partial Q_a}{\partial \hat{P}_{ij}} X_a + \Lambda^T\left[\frac{\partial F_a}{\partial \hat{P}_{ij}} X_a + X_a \frac{\partial F_a^T}{\partial \hat{P}_{ij}} + \frac{\partial}{\partial \hat{P}_{ij}}\left(G_a R_a G_a^T\right)\right]\right] \tag{B4}$$

where $\hat{P}_{ij}$ is a nonzero element of $\hat{P}$. Since Q_a is symmetric, equation (B3) leads to Lyapunov equation (20) which is dual to equation (11) and can be solved to obtain Λ. Thus, Λ is also symmetric. Equation (B4) represents $M(M + N_O + N_C)$ equations for $\partial J/\partial \hat{P}_{ij}$. Since equation (B4) cannot be solved explicitly for $\hat{P}$, one can use it to express the gradients of J with respect to $\hat{P}_{ij}$ as follows. Since R_a, Q_a, and Λ are symmetric, the trace properties of compatible matrix products can be used to write equation (B4) as

$$\frac{\partial J}{\partial \hat{P}_{ij}} = \mathrm{tr}\left[\frac{\partial Q_a}{\partial \hat{P}_{ij}} X_a + 2\frac{\partial F_a}{\partial \hat{P}_{ij}} X_a\Lambda + 2\frac{\partial G_a}{\partial \hat{P}_{ij}} R_a G_a^T\Lambda\right] \tag{B5}$$

subject to equation (11).

APPENDIX B

In order to express F_a, Q_a, and G_a explicitly in terms of $\hat{P}$, rewrite

$$\left.\begin{aligned} F_a &= \hat{F} + \hat{G}\hat{P}\hat{H} \\ Q_a &= \hat{Q}_1 + \hat{H}^T\hat{P}^T\hat{Q}_2\hat{P}\hat{H} \\ G_a &= \hat{G}_w + \hat{G}\hat{P}\hat{I} \end{aligned}\right\} \tag{B6}$$

where

$$\left.\begin{aligned} \hat{F} &= \left[\begin{array}{c|c} F & 0 \\ \hline 0 & 0 \end{array}\right]_{(N_S+M)\times(N_S+M)} & \hat{G} &= \left[\begin{array}{c|c} G_u & 0 \\ \hline 0 & I \end{array}\right]_{(N_S+M)\times(N_C+M)} \\ \hat{H} &= \left[\begin{array}{c|c} H & 0 \\ \hline 0 & I \end{array}\right]_{(N_O+M)\times(N_S+M)} & \hat{G}_w &= \left[\begin{array}{c|c} G_w & 0 \\ \hline 0 & 0 \end{array}\right]_{(N_S+M)\times(N_w+N_O)} \\ \hat{Q}_1 &= \left[\begin{array}{c|c} H_D^T Q_1 H_D & \\ \hline 0 & 0 \end{array}\right]_{(N_S+M)\times(N_S+M)} & \hat{Q}_2 &= \left[\begin{array}{c|c} Q_2 & 0 \\ \hline 0 & 0 \end{array}\right]_{(N_C+M)\times(N_C+M)} \\ \hat{I} &= \left[\begin{array}{c|c} 0 & I \\ \hline 0 & 0 \end{array}\right]_{(N_O+M)\times(N_w+N_O)} \end{aligned}\right\} \tag{B7}$$

One can now write equation (B5) as

$$\frac{\partial J}{\partial \hat{P}_{ij}} = \mathrm{tr}\left[\frac{\partial\left(\hat{H}^T\hat{P}^T\hat{Q}_2\hat{P}\hat{H}\right)}{\partial \hat{P}_{ij}} X_a + 2\,\frac{\partial(\hat{G}\hat{P})}{\partial \hat{P}_{ij}}\left(\hat{H}X_a\Lambda\right) + 2\,\frac{\partial(\hat{G}\hat{P})}{\partial \hat{P}_{ij}}\left(\hat{I}R_aG_a^T\Lambda\right)\right]$$

$$\frac{\partial J}{\partial \hat{P}_{ij}} = \mathrm{tr}\left[\hat{H}^T \frac{\partial\left(\hat{P}^T\hat{Q}_2\hat{P}\right)}{\partial \hat{P}_{ij}} \hat{H}X_a + 2\left(\hat{H}X_a\Lambda\right)\frac{\partial(\hat{G}\hat{P})}{\partial \hat{P}_{ij}} + 2\left(\hat{I}R_aG_a{}^T\Lambda\right)\frac{\partial(\hat{G}\hat{P})}{\partial \hat{P}_{ij}}\right]$$

$$= \mathrm{tr}\left[\frac{\partial\left(\hat{P}^T\hat{Q}_2\hat{P}\right)}{\partial \hat{P}_{ij}}\left(\hat{H}X_a\hat{H}^T\right) + 2\,\frac{\partial\left(\hat{P}^T\hat{G}^T\right)}{\partial \hat{P}_{ij}}\left(\Lambda X_a\hat{H}^T\right) + 2\,\frac{\partial\left(\hat{P}^T\hat{G}^T\right)}{\partial \hat{P}_{ij}}\left(\Lambda G_aR_a\hat{I}^T\right)\right] \tag{B8}$$

Collecting the derivatives with respect to all the $\hat{P}_{ij}$'s results in

$$\frac{\partial J}{\partial \hat{P}} = 2\left[\hat{Q}_2\hat{P}\left(\hat{H}X_a\hat{H}^T\right) + \hat{G}^T\left(\Lambda X_a\hat{H}^T\right) + \hat{G}^T\left(\Lambda G_aR_a\hat{I}^T\right)\right] \tag{B9}$$

Note that in equation (B9), both the left and right terms represent $(N_C + M) \times (N_O + M)$ matrices. Hence, the evaluation of the trace for derivatives with respect to each $\hat{P}_{ij}$ is no longer required. By expanding equation (B9) by using equations (12), (19), and (B7), equations (16) to (18) are obtained.

APPENDIX C

SIGNIFICANCE OF A, B, AND C FOR FULL-ORDER CONTROLLER

For a full-order controller (i.e., $M = N_S$ and $R = I$), if we set

$$A = F - BH + G_u C \tag{C1}$$

and use B and C as design variables, then equations (26) can be expressed as

$$\frac{dJ}{dB} = \Lambda_c\left(BR_v - PH^T\right) + \left(\Lambda_{sc}^T + \Lambda_c\right)\left(X_s - X_{sc}\right)H^T \tag{C2}$$

$$\frac{dJ}{dC} = \left(Q_2 C + G_u^T S\right)X_c + G_u^T\left(\Lambda_s + \Lambda_{sc}^T\right)\left(X_{sc} - X_c\right) \tag{C3}$$

where

$$P = \left(X_s + X_c - X_{sc} - X_{sc}^T\right) = E\left[ee^T\right] \tag{C4}$$

$$S = \left(\Lambda_s + \Lambda_c + \Lambda_{sc} + \Lambda_{sc}^T\right) \tag{C5}$$

$$e = \left(x_c - x_s\right) \tag{C6}$$

Here P is recognized as the steady-state covariance matrix of the estimation error e. From equations (11) and (20), one can show that P and S satisfy a set of Lyapunov equations as follows.

Partition equation (11) into four $N_S \times N_S$ blocks, i.e.,

$$\left[\begin{array}{c|c} F & G_u C \\ \hline BH & A \end{array}\right]\left[\begin{array}{c|c} X_s & X_{sc} \\ \hline X_{sc}^T & X_c \end{array}\right] + \left[\begin{array}{c|c} X_s & X_{sc} \\ \hline X_{sc}^T & X_c \end{array}\right]\left[\begin{array}{c|c} F & G_u C \\ \hline BH & A \end{array}\right]^T + \left[\begin{array}{c|c} G_w R_w G_w^T & 0 \\ \hline 0 & BR_v B^T \end{array}\right] = 0 \tag{C7}$$

Equation (C7) represents four sets of matrix equations:

$$FX_S + G_uCX_{SC}^T + X_SF^T + X_{SC}C^TG_u^T + G_wR_wG_w^T = 0 \quad \text{(C8)}$$

$$FX_{SC} + G_uCX_C + X_SH^TB^T + X_{SC}A^T = 0 \quad \text{(C9)}$$

$$BHX_S + AX_{SC}^T + X_{SC}^TF^T + X_CC^TG_u^T = 0 \quad \text{(C10)}$$

$$BHX_{SC} + AX_C + X_{SC}^TH^TB^T + X_CA^T + BR_VB^T = 0 \quad \text{(C11)}$$

Similarly, equation (20) can be expressed in a partitioned form as

$$\left[\begin{array}{c|c} F & G_uC \\ \hline BH & A \end{array}\right]^T \left[\begin{array}{c|c} \Lambda_S & \Lambda_{SC} \\ \hline \Lambda_{SC}^T & \Lambda_C \end{array}\right] + \left[\begin{array}{c|c} \Lambda_S & \Lambda_{SC} \\ \hline \Lambda_{SC}^T & \Lambda_C \end{array}\right] \left[\begin{array}{c|c} F & G_uC \\ \hline BH & A \end{array}\right] + \left[\begin{array}{c|c} H_D^TQ_1H_D & 0 \\ \hline 0 & C^TQ_2C \end{array}\right] = 0 \quad \text{(C12)}$$

Because of symmetry, equations (C9) and (C10) represent the same set of equations. By substituting equation (C1) for A and subtracting both (C9) and (C10) from the sum of equations (C8) and (C11), all G_uC terms cancel and the following equation is obtained:

$$(F - BH)P + P(F - BH)^T + G_wR_wG_w^T + BR_VB^T = 0 \quad \text{(C13)}$$

By substituting equation (C1) for A and adding all four sets of matrix equations represented by equation (C12), all BH terms cancel and the following equation is obtained:

$$\left(F + G_uC\right)^TS + S\left(F + G_uC\right) + H_D^TQ_1H_D + C^TQ_2C = 0 \quad \text{(C14)}$$

From equations (C2) and (C3), it is easily seen that $dJ/dB = 0$ and $dJ/dC = 0$ provided that

$$B = PH^TR_V^{-1} \equiv B_O \quad \text{(C15)}$$

$$C = -Q_2^{-1} G_u^T S \equiv C_o \tag{C16}$$

and provided that

$$\left(X_c - X_{sc}\right) = 0 \tag{C17}$$

and

$$\left(\Lambda_c + \Lambda_{sc}^T\right) = 0 \tag{C18}$$

which is indeed true as shown below.

Subtracting equation (C11) from equation (C9), one obtains

$$(F - BH)\left(X_{sc} - X_c\right) + \left(X_{sc} - X_c\right)\left(F + G_u C\right)^T + \left(PH^T - BR_v\right)B^T = 0 \tag{C19}$$

Adding the last two sets of partitioned equations (C12), one obtains

$$(F - BH)^T\left(\Lambda_{sc}^T + \Lambda_c\right) + \left(\Lambda_{sc}^T + \Lambda_c\right)\left(F + G_u C\right) + C^T\left(G_u^T S + Q_2 C\right) = 0 \tag{C20}$$

If equations (C15) and (C16) are satisfied, then equations (C19) and (C20) are homogeneous equations in $\left(X_{sc} - X_c\right)$ and $\left(\Lambda_{sc}^T + \Lambda_c\right)$, respectively, and can have only a trivial solution provided that $(F - BH)$ and $-(F + G_u C)$ have no eigenvalues in common. Hence equations (C17) and (C18) are satisfied. Equations (C15) and (C16) for B and C are recognized as the Kalman estimator gain and optimal full-state feedback gain matrices, respectively, as given by the LQG solution.

It is also recognized that equation (C17) implies that

$$E\left[ex_c^T\right] = 0 \tag{C21}$$

i.e., the estimation error and the estimated states are uncorrelated, an important result in optimal filtering and prediction. Substituting equations (C15) and (C16) into equations (C13) and (C14), respectively, results in the steady-state Riccati equations for computing P and S:

$$FP + PF^T - PH^T R_v^{-1} HP + G_w R_w G_w^T = 0 \tag{C22}$$

$$F^T S + SF - SG_u Q_2^{-1} G_u^T S + H_D^T Q_1 H_D = 0 \tag{C23}$$

Also from equations (C4) and (C17), the state covariance matrix is given by

$$X_S = P + X_C \tag{C24}$$

and the performance index given by equation (15) becomes

$$J = \mathrm{tr}\left[\left(H_D^T Q_1 H_D + C^T Q_2 C\right) X_C + \left(H_D^T Q_1 H_D\right) P\right] \tag{C25}$$

APPENDIX D

DISCUSSION OF ESTIMATION ERROR

For $M = N_s$, the states x_c of the controller discussed in this paper are optimal estimates of the plant states x_s as shown in appendix C. By analogy, for $M < N_s$, the controller states x_c may be treated as an estimate of M key plant states denoted by x_1. Let the remaining $N_s - M$ plant states be denoted by x_2. Rearranging and partitioning x_s and equations (4) and (5) accordingly, one can rewrite them as

$$\dot{x}_s = \begin{Bmatrix} \dot{x}_1 \\ \dot{x}_2 \end{Bmatrix} = \left[\begin{array}{c|c} F_{11} & F_{12} \\ \hline F_{21} & F_{22} \end{array}\right] \begin{Bmatrix} x_1 \\ x_2 \end{Bmatrix} + \left[\begin{array}{c|c} G_{u1} & G_{w1} \\ \hline G_{u2} & G_{w2} \end{array}\right] \begin{Bmatrix} u \\ w \end{Bmatrix} \tag{D1}$$

$$y = \left[\begin{array}{c|c} H_1 & H_2 \end{array}\right] \begin{Bmatrix} x_1 \\ x_2 \end{Bmatrix} + v \tag{D2}$$

where

$$x_1 \equiv Rx_s \qquad G_{w1} \equiv RG_w$$

$$F_{11} \equiv RFR^T \qquad H_1 \equiv HR^T$$

$$G_{u1} \equiv RG_u$$

Now defining the error e in the partial state estimation as

$$e \equiv x_c - x_1 \equiv x_c - Rx_s \tag{D3}$$

and subtracting the first M equations in equation (D1) from equation (7), one obtains the error dynamics equation as

$$\dot{e} = Ax_c - (F_{11} - BH_1)x_1 - (F_{12} - BH_2)x_2 - G_{u1}u - G_{w1}w + Bv \tag{D4}$$

If we let

$$A = F_{11} - BH_1 + G_{u1}C \tag{D5}$$

then equation (D4) becomes

$$\dot{e} = (F_{11} - BH_1)e - (F_{12} - BH_2)x_2 - G_{u1}(u - Cx_c) - G_{w1}w + Bv \tag{D6}$$

In the usual case, $(u - Cx_c)$ is set to zero as per equation (8). In the present design, to improve the robustness of the reduced-order controller, $(u - Cx_c)$ is replaced by a fictitious input white noise process η_u of intensity R_u (ref. 10). Thus,

$$\dot{e} = (F_{11} - BH_1)e - \underline{(F_{12} - BH_2)x_2} - G_{u1}\eta_u - G_{w1}w + Bv \tag{D7}$$

Thus η_u appears as an additional noise parameter in the error dynamics. The underlined terms contribute to additional estimation error apart from the white noise inputs. These terms are referred to as observation spillover terms in reference 16, in which use of a prefilter is suggested to eliminate them.

If $(F_{11} - BH_1)$ is stable in equation (D7) and F_a (eq. (10)) is stable for a specific choice of B and C, then e is stable and asymptotically converges to a steady-state value.

REFERENCES

1. Abel, Irving; Newsom, Jerry R.; and Dunn, Henry J.: Application of Two Synthesis Methods for Active Flutter Suppression on an Aeroelastic Wind-Tunnel Model. A Collection of Technical Papers - AIAA/Atmospheric Flight Mechanics Conference for Future Space Systems, Aug. 1979, pp. 93-103. (Available as AIAA Paper 79-1633.)

2. Abel, Irving: An Analytical Technique for Predicting the Characteristics of a Flexible Wing Equipped With an Active Flutter-Suppression System and Comparison With Wind-Tunnel Data. NASA TP-1367, 1979.

3. Roger, Kenneth L.: Airplane Math Modeling Methods for Active Control Design. Structural Aspects of Active Controls, AGARD-CP-228, Aug. 1977, pp. 4-1 - 4-11.

4. Gangsaas, Dagfinn; and Ly, Uy-Loi: Application of a Modified Linear Quadratic Gaussian Design to Active Control of a Transport Airplane. AIAA Paper 79-1746, Aug. 1979.

5. Newsom, Jerry R.: A Method for Obtaining Practical Flutter-Suppression Control Laws Using Results of Optimal Control Theory. NASA TP-1471, 1979.

6. Mahesh, J. K.; Garrard, W. L.; Stone, C. R.; and Hausman, P. D.: Active Flutter Control for Flexible Vehicles. Volume 1 - Final Report. NASA CR-159160, 1979.

7. Kwakernaak, Huibert; and Sivan, Raphael: Linear Optimal Control Systems. John Wiley & Sons, Inc., c.1972, pp. 427-434.

8. Levine, William S.; Johnson, Timothy L.; and Athans, Michael: Optimal Limited State Variable Feedback Controllers for Linear Systems. IEEE Trans. Autom. Control, vol. AC-16, no. 6, Dec. 1971, pp. 785-793.

9. Martin, Gary Don; and Bryson, Arthur E., Jr.: Attitude Control of a Flexible Spacecraft. A Collection of Technical Papers - AIAA Guidance and Control Conference, Aug. 1978, pp. 281-287. (Available as AIAA Paper 78-1281.)

10. Doyle, J. C.; and Stein, G.: Robustness With Observers. IEEE Trans. Autom. Control, vol. AC-24, no. 4, Aug. 1979, pp. 607-611.

11. Albano, Edward; and Rodden, William P.: A Doublet-Lattice Method for Calculating Lift Distributions on Oscillating Surfaces in Subsonic Flows. AIAA J., vol. 7, no. 2, Feb. 1969, pp. 279-285; Errata, vol. 7, no. 11, Nov. 1969, p. 2192.

12. Denery, Dallas G.: Identification of System Parameters From Input-Output Data With Application to Air Vehicles. NASA TN D-6468, 1971.

13. Vanderplaats, Garret N.: CONMIN - A Fortran Program for Constrained Function Minimization. User's Manual. NASA TM X-62282, 1973.

14. Armstrong, Ernest S.: ORACLS - A Design System for Linear Multivariable Control. Marcel Dekker, Inc., c.1980.

15. Mukhopadhyay, V.; Newsom, J. R.; and Abel, I.: A Direct Method for Synthesizing Low-Order Optimal Feedback Control Laws With Application to Flutter Suppression. A Collection of Technical Papers - AIAA Atmospheric Flight Mechanics Conference, Aug. 1980, pp. 465-475. (Available as AIAA-80-1613.)

16. Balas, M. J.: Active Control of Flexible Systems. J. Optimization Theory & Appl., vol. 25, no. 3, July 1978, pp. 415-436.

SYMBOLS

A	controller dynamics matrix
A^*_{ac}	dynamics matrix of actuator
A^*_G	dynamics matrix of turbulence
$\left[\hat{A}_n\right], \left[\hat{B}_m\right]$	matrices for polynomial fit (eq. (2))
$\left[\hat{A}_n\right]_C, \left[\hat{B}_m\right]_C$	control surface component of $\left[\hat{A}_n\right]$ and $\left[\hat{B}_m\right]$
$\left[\hat{A}_n\right]_F, \left[\hat{B}_m\right]_F$	modal component of $\left[\hat{A}_n\right]$ and $\left[\hat{B}_m\right]$
$\left[\hat{A}_n\right]_G, \left[\hat{B}_m\right]_G$	gust component of $\left[\hat{A}_n\right]$ and $\left[\hat{B}_m\right]$
B	controller input matrix
B^*_{ac}	control distribution matrix of actuator
B^*_G	control distribution matrix of turbulence
B_o	Kalman estimator gain matrix
C	controller output matrix
C^*_{ac}	output matrix of actuator
C^*_G	output matrix of turbulence
C_o	optimal full-state feedback gain matrix
c	reference chord length
$\left[D_s\right]$	structural damping matrix
e	estimation error vector
F	plant dynamics matrix
F_a	augmented dynamics matrix
$F_{11}, F_{12}, \ldots$	components of partitioned matrix F
F^*	dynamics matrix for equation (1)
$\hat{F}$	matrix defined in equations (B7)
G_a	augmented noise input matrix

G_u	plant input matrix
G_{u1}, G_{u2}	components of partitioned matrix G_u (eq. (D1))
G_w	gust input matrix
G_{w1}, G_{w2}	components of partitioned matrix G_w (eq. (D1))
$\hat{G}, \hat{G}_w$	matrices defined in equations (B7)
G_1^*, G_2^*	input matrices in equations (3a) and (A7)
g	gravitational acceleration
H	sensor output matrix
H_D	design output matrix
H_1, H_2	components of partitioned matrix H (eq. (D2))
$\hat{H}$	matrix defined in equations (B7)
H_1^*, H_2^*, H_3^*	measurement matrices in equations (3b) and (A9)
I	unity matrix
$\hat{I}$	matrix defined in equations (B7)
J	performance index
[K]	generalized stiffness matrix
L	number of aerodynamic lag terms
ℓ	scale of turbulence
M	order of controller
[M]	generalized mass matrix
N_C	number of control inputs
N_D	number of design outputs
N_O	number of outputs or sensors
N_S	number of plant states
N_W	number of plant noise inputs

P	Kalman estimator error covariance matrix
$\hat{P}$	matrix defined in equation (B2)
$\hat{P}_{ij}$	nonzero elements of $\hat{P}$ matrix
Q_a	augmented symmetric weighting matrix
Q_1	design output symmetric weighting matrix
Q_2	control input symmetric weighting matrix
$\left[\hat{Q}\right], \left[\hat{Q}\right]_G$	s-plane approximation of unsteady aerodynamics matrices
$\hat{Q}_1, \hat{Q}_2$	matrices defined in equations (B7)
q	dynamic pressure
q_f	flutter dynamic pressure
R	key state selection matrix
R_a	augmented noise intensity matrix
R_u	fictitious input-noise intensity matrix
R_v	measurement noise intensity matrix
R_w	plant noise intensity matrix
S	full-state feedback optimal solution matrix
s	Laplace variable
t	time
U	input covariance matrix (steady state)
u	control input vector
u^*	input vector for equation (1)
V	free-stream velocity
v	measurement noise vector
w	plant noise vector
X_a	covariance matrix of augmented state vector (steady state)
X_s, X_c, X_{sc}	components of partitioned matrix X_a (eq. (12))

x_a augmented state vector

x_c controller state vector

x_s augmented plant state vector

x_1 vector of key plant states to be estimated

x_2 vector of plant states not estimated

x^* state vector for equation (1)

x^*_{ac} actuator state vector

$x^*_{F_1}$ generalized coordinate vector

$x^*_{F_2}$ time derivative of generalized coordinate vector

x^*_G turbulence state vector

$x^*_{\beta_1},\ldots,x^*_{\beta_L}$ aerodynamic states

y measurement output vector

y_D design output vector

$\ddot{z}$ accelerometer output

β_m aerodynamic lag

δ control surface deflection

$\dot{\delta}$ control surface deflection rate

δ_c commanded control surface deflection

η augmented noise vector

η_u fictitious input-noise vector

Λ Lagrange multiplier matrix

$\Lambda_s,\Lambda_c,\Lambda_{sc}$ components of partitioned matrix Λ (eq. (19))

ξ_C generalized coordinate vector for control surface deflection

ξ_F generalized coordinate vector for flexible modes

ξ_G gust velocity vector

σ_{wg} root-mean-square gust velocity

Φ matrix of modal amplitudes at sensor location

Subscript:

rms root mean square

Mathematical notation:

E[ ] expected value of

tr[ ] trace of matrix

$\equiv$ defined as

[ ] matrix

{ } vector

$[\ ]^T$ vector or matrix transpose

$[\ ]^{-1}$ inverse of square matrix

Dots over symbols denote differentiation with respect to time.

TABLE I.- SUMMARY OF RESULTS FOR 25TH-ORDER PLANT

$[Q_1 = 0.0001, \quad Q_2 = 50000, \quad H = H_D, \quad R_w = 1.0, \quad R_v = 1.0, \quad q = 7.66 \text{ kPa}]$

Order of controller, M	Design input noise intensity, R_u	Optimal performance index, J	Steady-state responses with $R_u = 0$				Gain margin			Phase margin				Flutter dynamic pressure, q_f, kPa
			u_{rms}, deg	δ_{rms}, deg	$\dot{\delta}_{rms}$, deg/sec	$\ddot{z}_{rms}$, g units	dB	rad/sec	dB	rad/sec	deg	rad/sec	deg	rad/sec	
Full	0	1.64	11.8	11.8	842.5	5.35	-4.3	66	2.2	132	-44	53	18	91	
	.00001	51.3	21.5	18.0	795.3	3.12	-5.7	60	18.9	616	-47	46	65	82	9.0
	.0001	454.0	37.6	19.4	843.7	2.83	-6.1	60	21.5	860	-51	44	72	84	
4	0	1.77	12.6	12.6	696.8	4.88	-4.1	63	2.6	120	-41	52	22	92	
	.00001	59.5	17.2	17.0	756.0	3.52	-5.0	60	12.3	314	-46	47	53	83	8.7
	.0001	574.9	18.1	18.0	757.1	3.46	-5.0	61	12.3	305	-51	46	55	82	

TABLE II.- COMPARISON OF RESULTS WITH CONTROLLERS DESIGNED BY VARIOUS METHODS FOR 25TH-ORDER PLANT

$[Q_1 = 0.0001, \quad Q_2 = 50000, \quad H = H_D, \quad R_w = 1.0, \quad R_v = 1.0, \quad q = 7.66 \text{ kPa}]$

Controller design method	Order of controller, M	Design input noise intensity, R_u	Optimal performance index, J	Steady-state responses with $R_u = 0$			Gain margin				Phase margin			
				δ_{rms}, deg	$\dot{\delta}_{rms}$, deg/sec	$\ddot{z}_{rms}$, g units	dB	rad/sec	dB	rad/sec	deg	rad/sec	deg	rad/sec
LQG	Full	0.00001	51.3	18.0	795.3	3.12	-5.7	60	18.9	616	-47	46	65	82
Truncation	4	.00001	110.9	32.6	1263.7	2.39	-10.3	59	6.5	254	-17	38	57	129
Residualization	4	.00001	85.5	17.1	665.4	2.82	-7.1	62	6.0	164	-55	46	38	97
Reoptimization (present method)	4	.00001	59.5	17.0	756.0	3.52	-5.0	60	12.3	314	-46	47	53	83

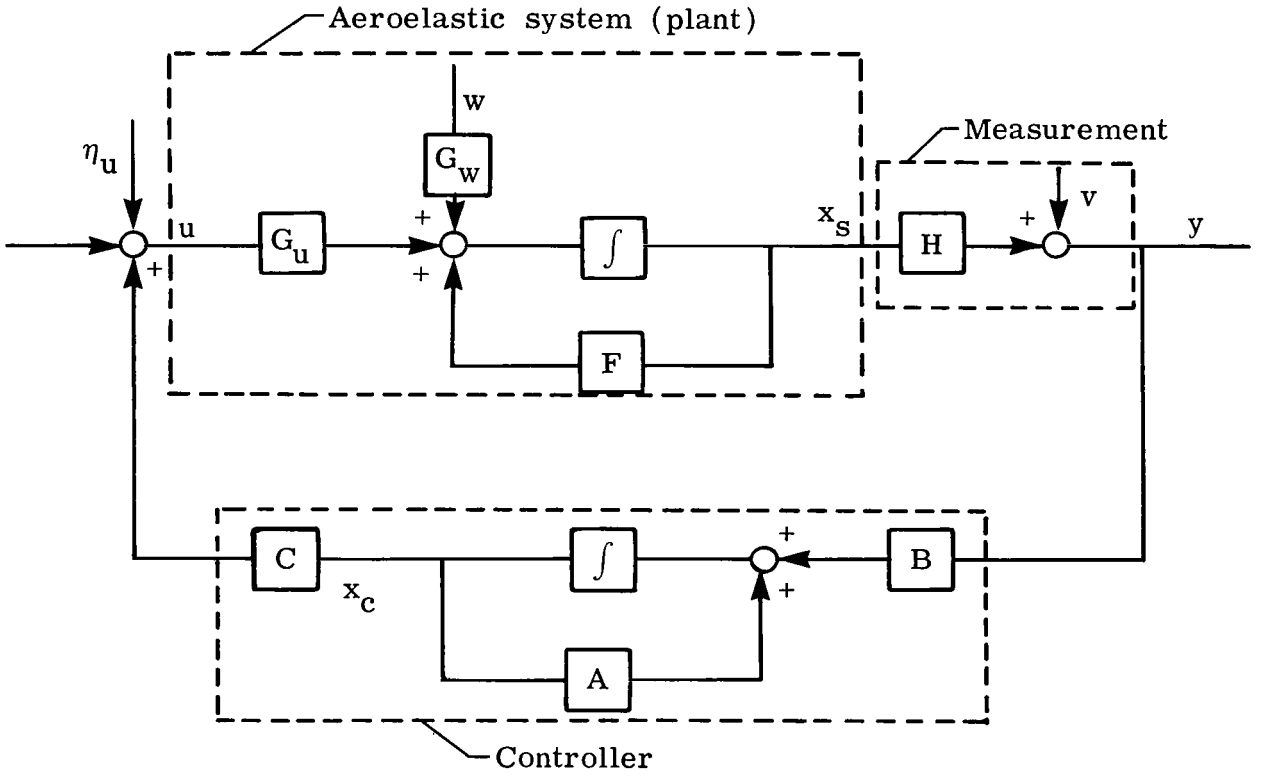

Figure 1.- Block diagram of the control scheme.

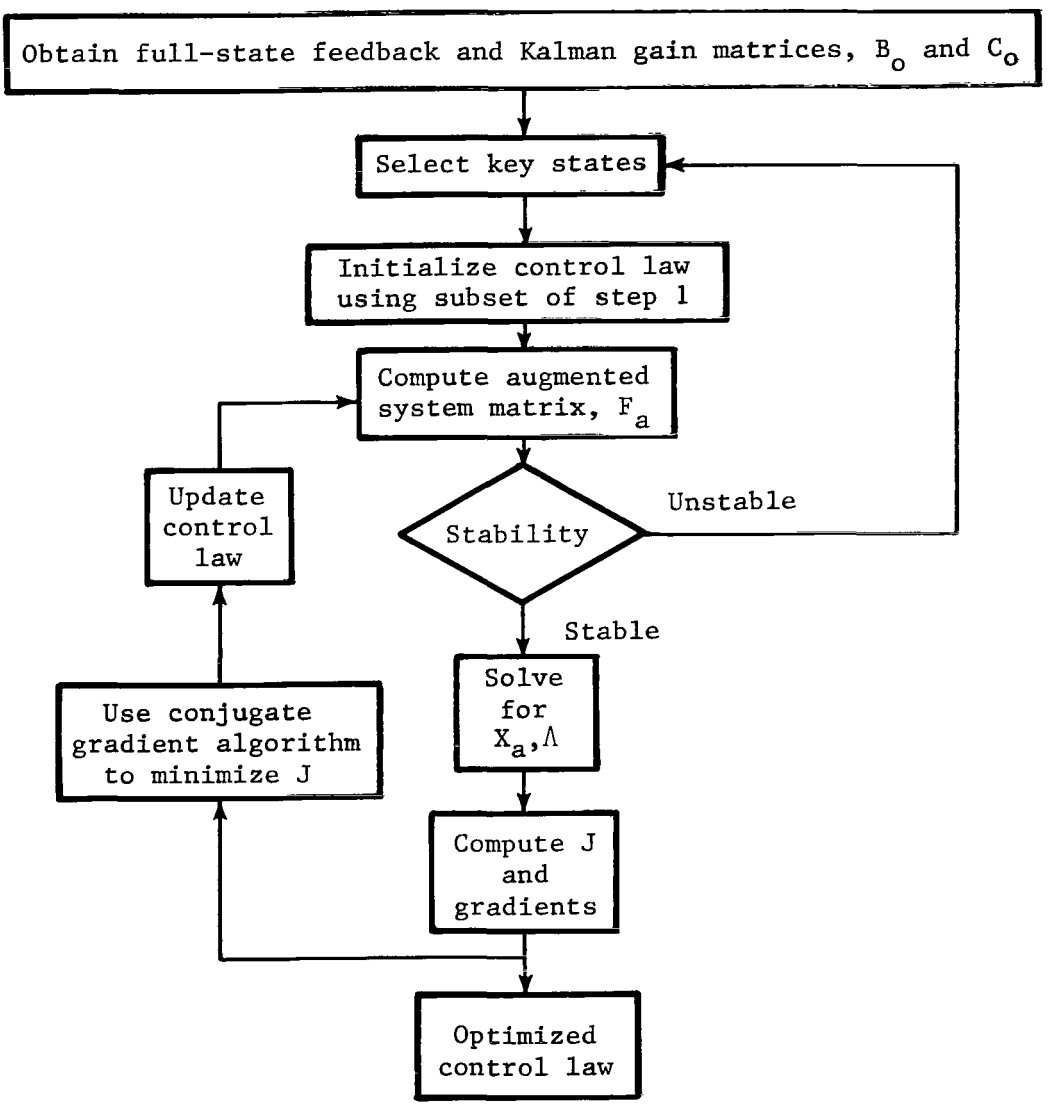

Figure 2.- Block diagram of design algorithm.

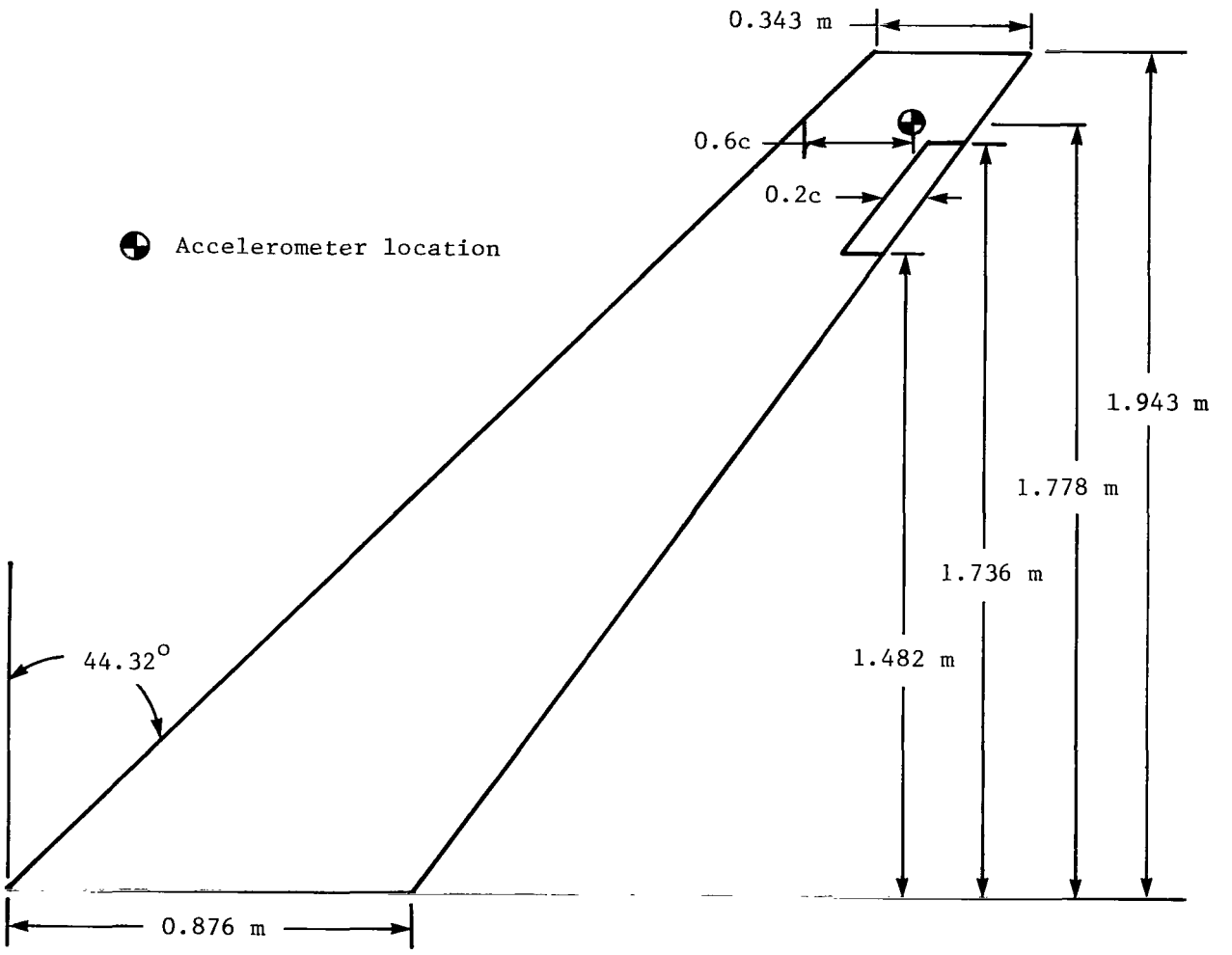

Figure 3.- Model geometry, sensor and control surface locations.

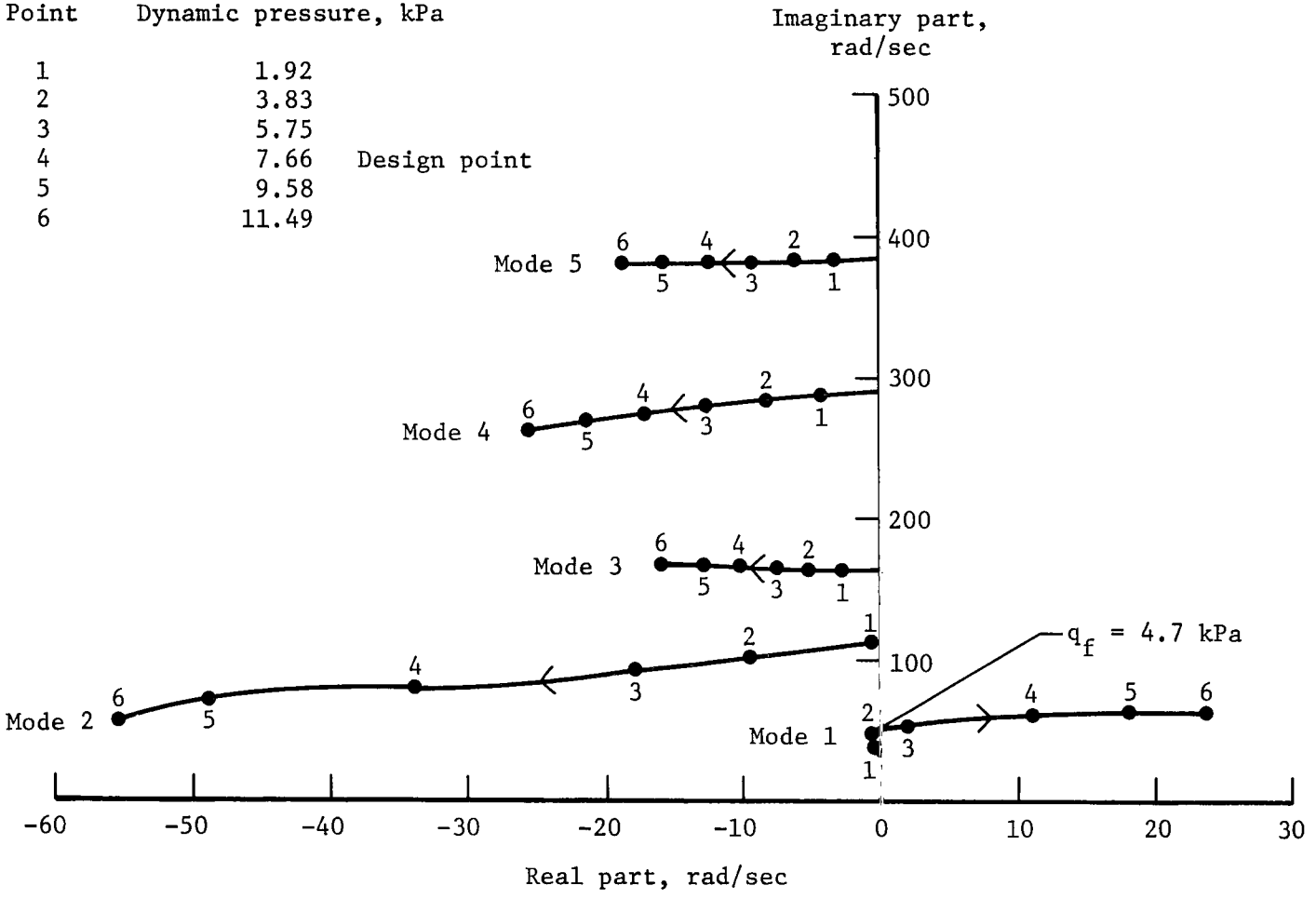

Figure 4.- Open-loop dynamic pressure root locus at Mach 0.9.

Point	Phase margin
A	-44^{o} at 53 rad/sec
B	$+18^{o}$ at 91 rad/sec
	Gain margin
C	-4.3 dB at 66 rad/sec
D	+2.2 dB at 132 rad/sec

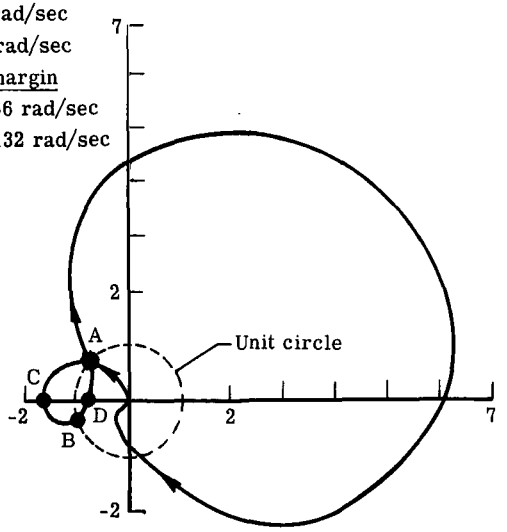

(a) $R_u = 0.$

Point	Phase margin
A	-47^{o} at 46 rad/sec
B	$+65^{o}$ at 82 rad/sec
	Gain margin
C	-5.7 dB at 60 rad/sec
D	+18.9 dB at 616 rad/sec

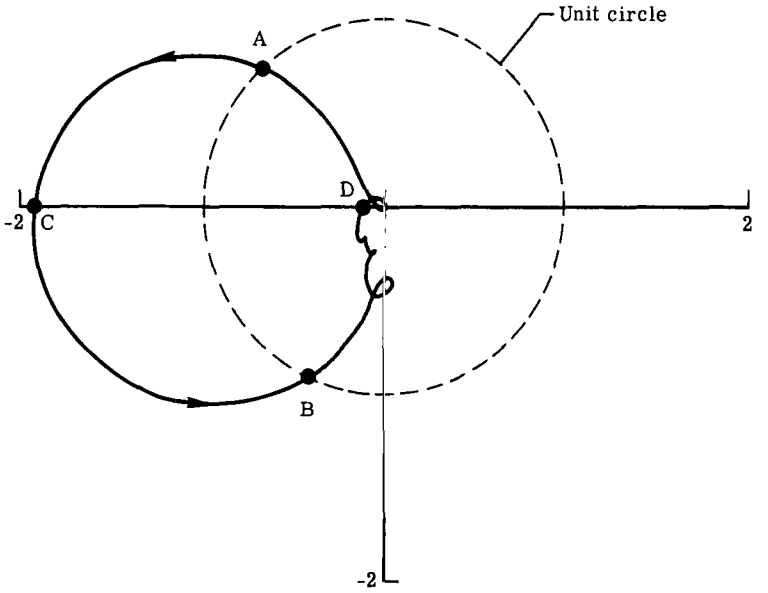

(b) $R_u = 0.00001.$

Figure 5.- Nyquist diagrams of plant plus full-order control law (arrows indicate increasing frequency). q = 7.66 kPa.

Point	Phase margin
A	-51^{o} at 44 rad/sec
B	$+72^{o}$ at 84 rad/sec
	Gain margin
C	-6.1 dB at 60 rad/sec
D	+21.5 dB at 860 rad/sec

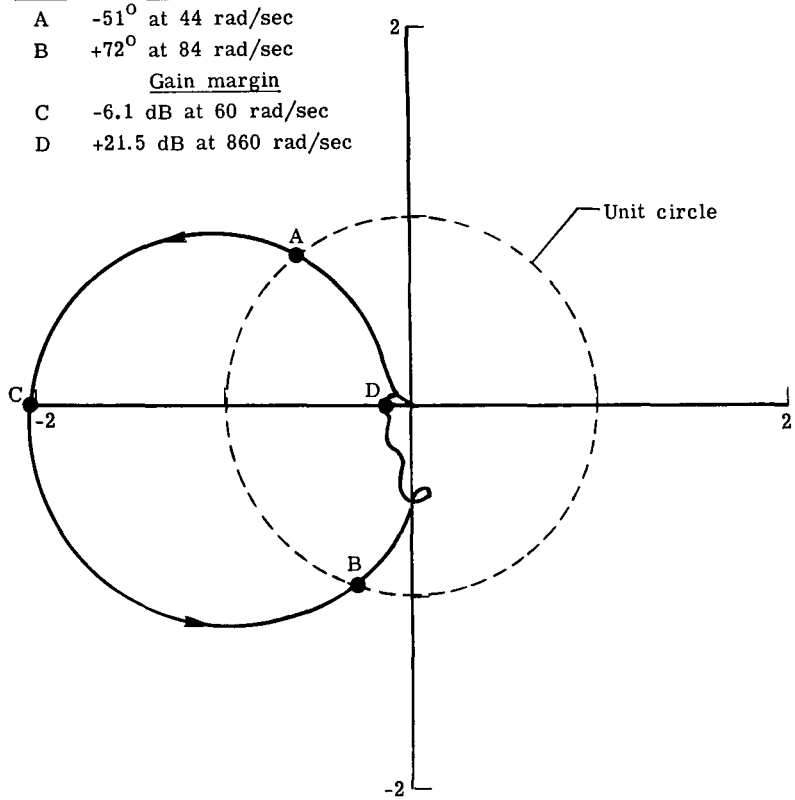

(c) $R_u = 0.0001$.

Figure 5.- Concluded.

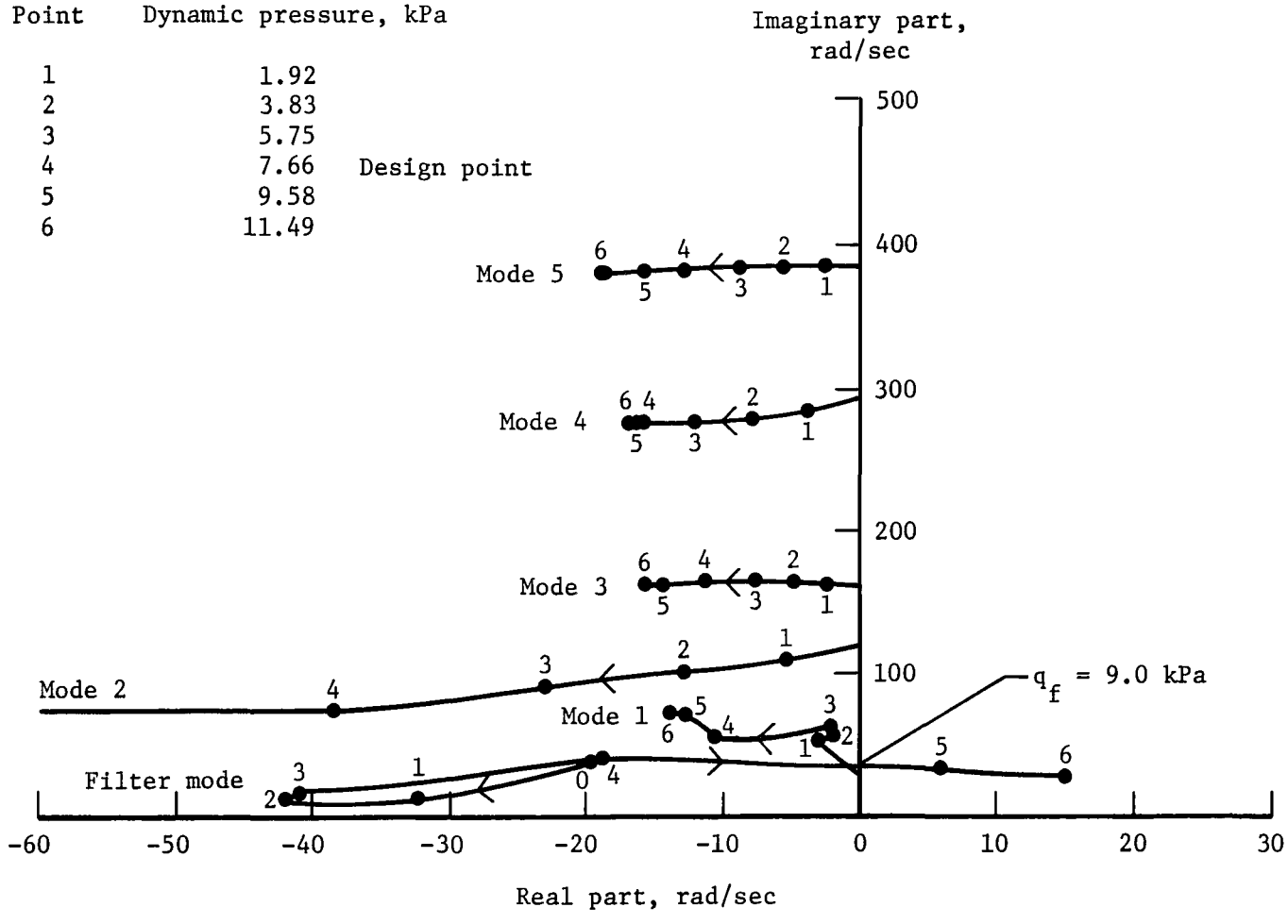

Figure 6.- Closed-loop dynamic-pressure root locus using full-order control law. R_u = 0.00001.

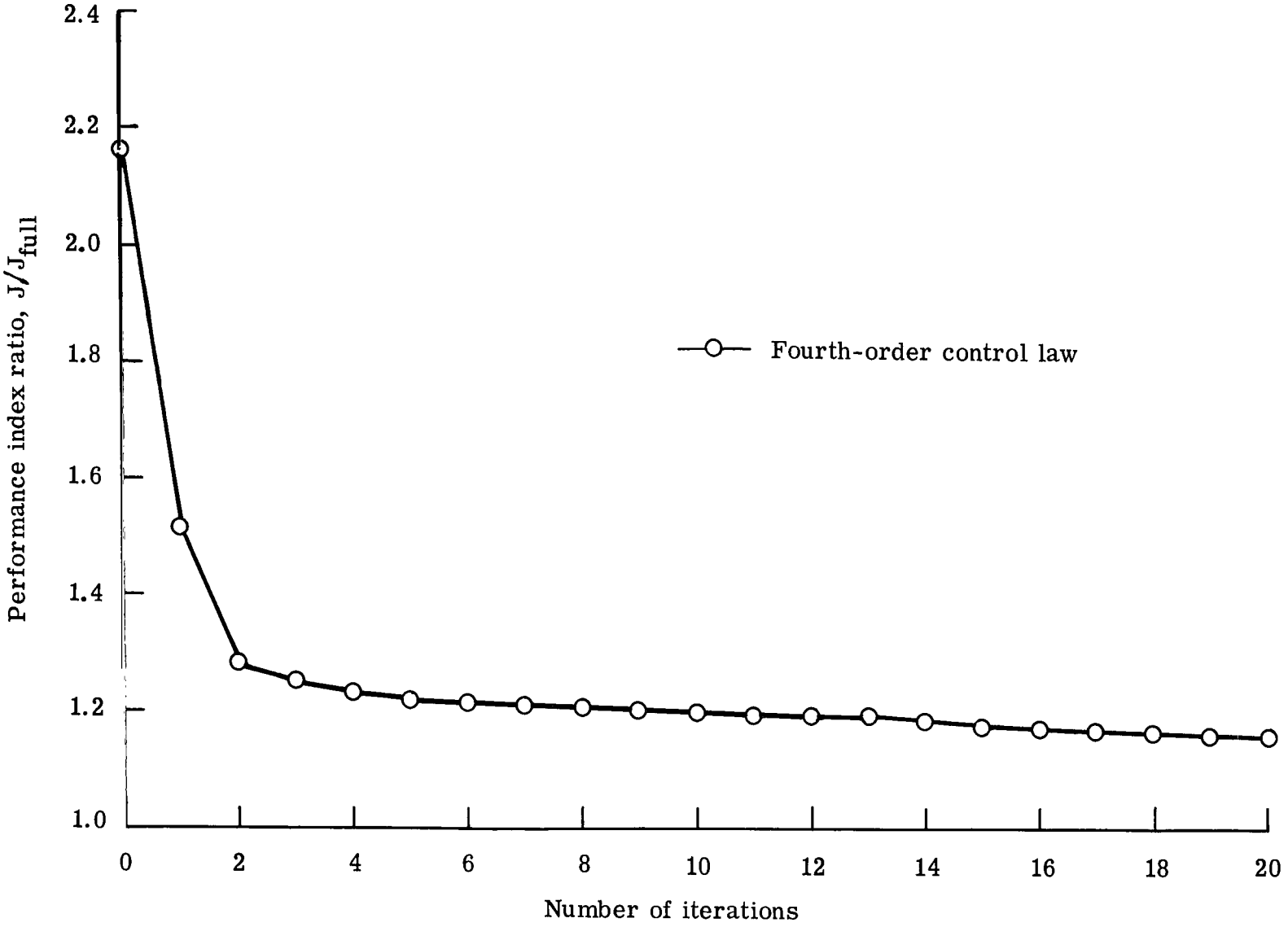

Figure 7.- Typical convergence pattern of performance index using a conjugate gradient algorithm. $R_u = 0.00001$.

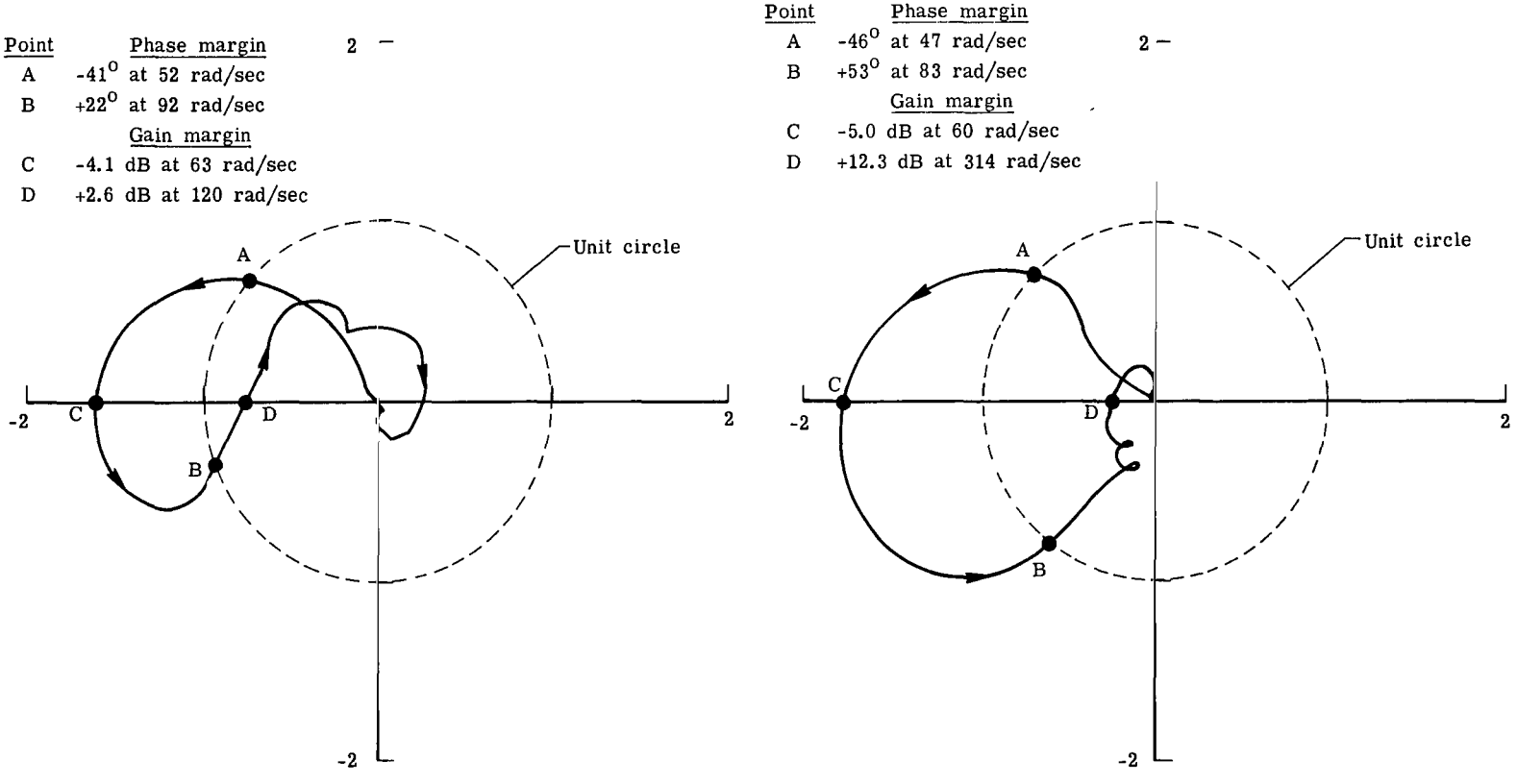

(a) $R_u = 0.$ (b) $R_u = 0.00001.$

Figure 8.- Nyquist diagrams of plant plus fourth-order control law (arrows indicate increasing frequency). q = 7.66 kPa.

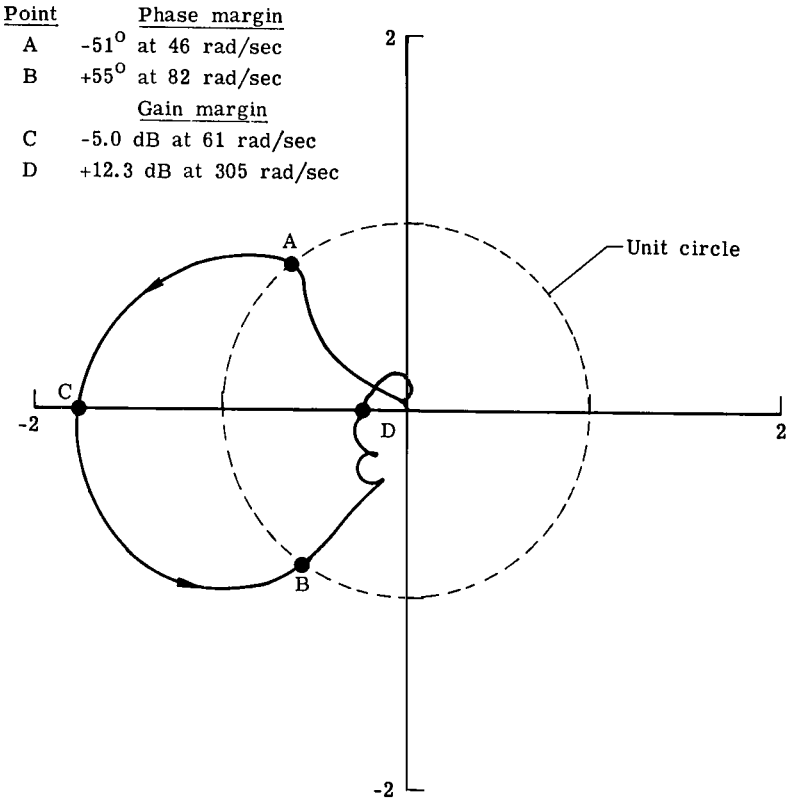

(c) $R_u = 0.0001$.

Figure 8.- Concluded.

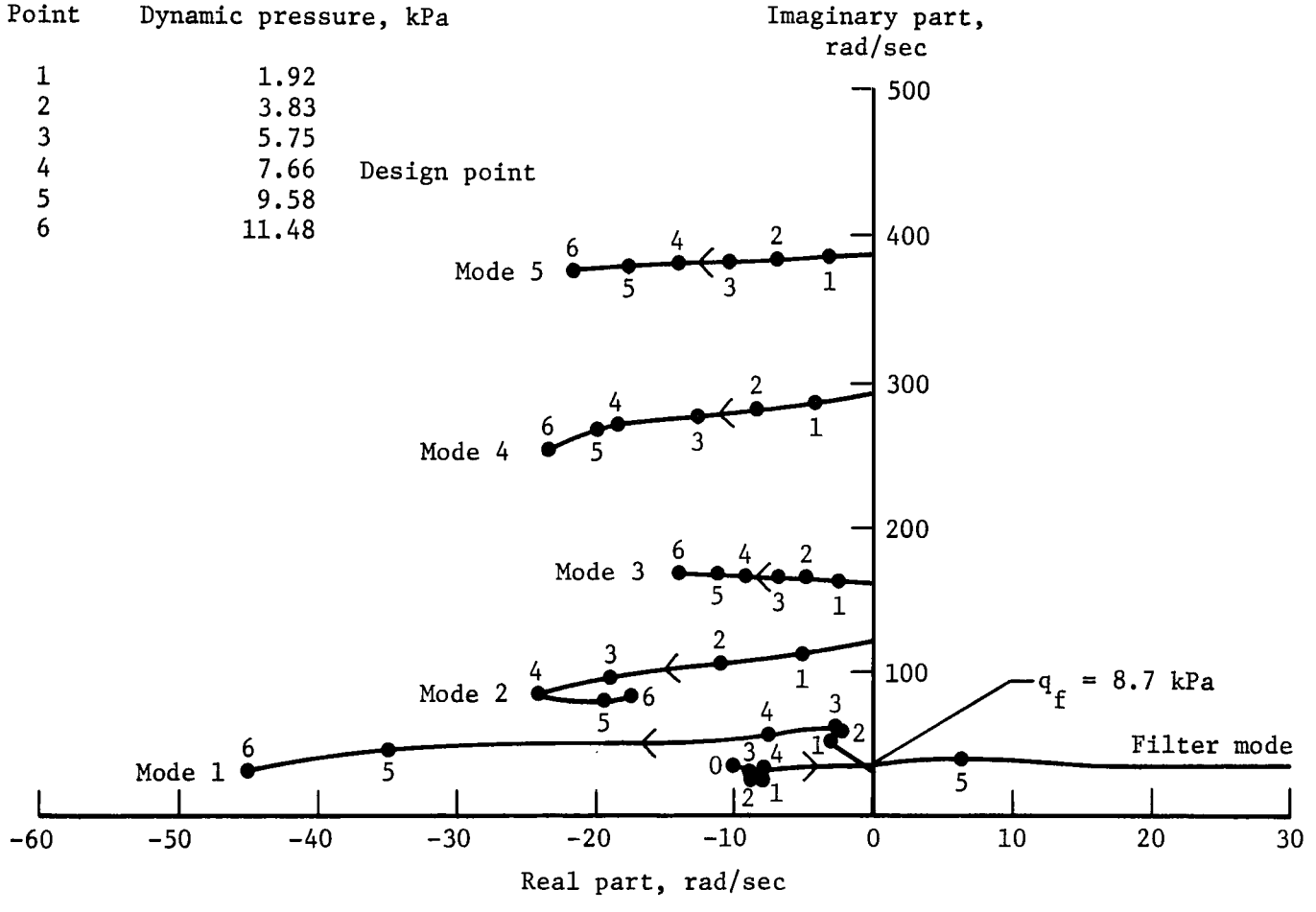

Figure 9.- Closed-loop dynamic-pressure root locus using fourth-order control law. R_u = 0.00001.

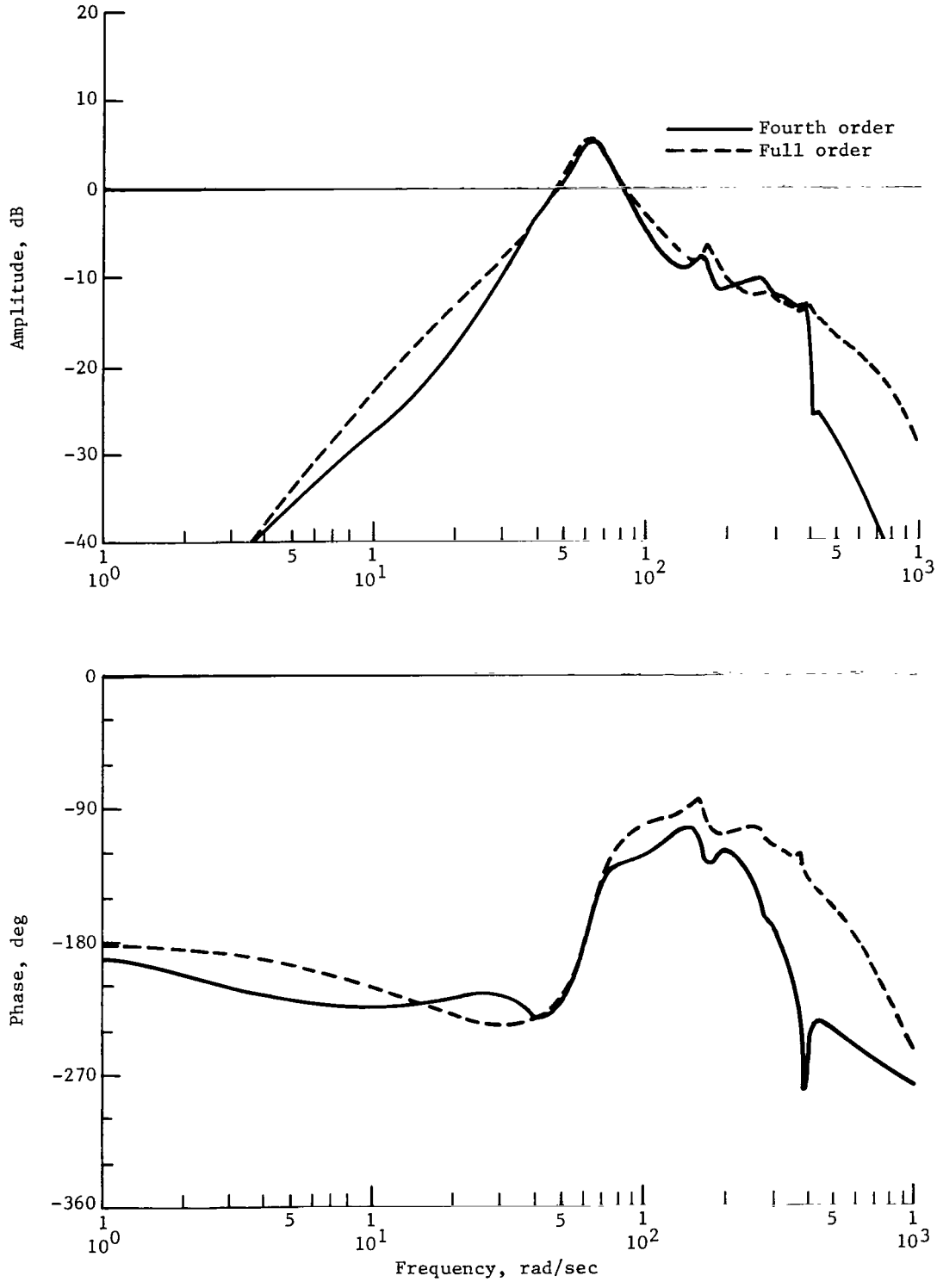

Figure 10.- Bode plot of plant plus full-order and fourth-order control laws at q = 7.66 kPa. R_u = 0.00001.

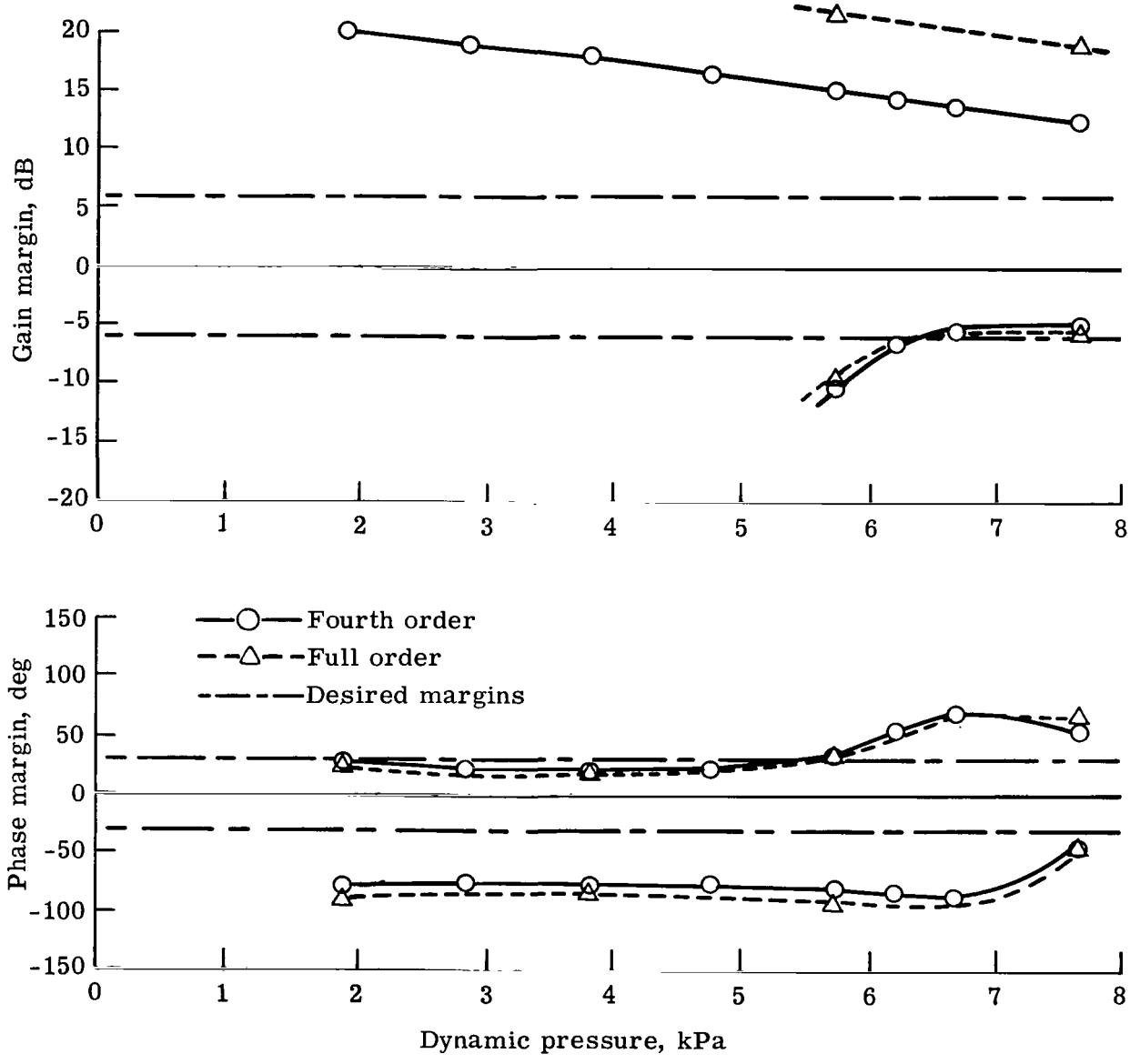

Figure 11.- Variation of stability margins with dynamic pressure for plant plus full-order and fourth-order control laws.

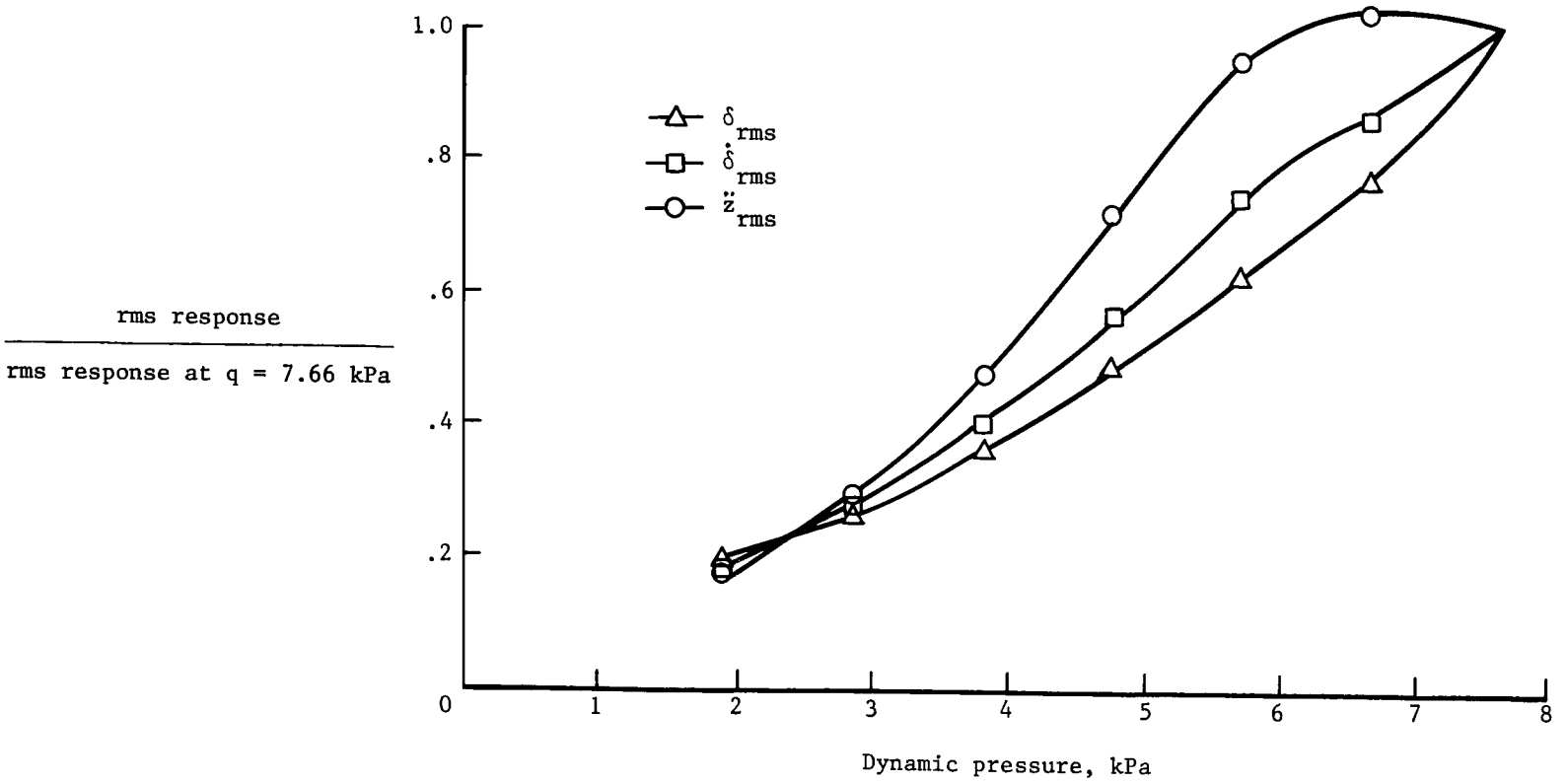

Figure 12.- Variation of steady-state root-mean-square (rms) responses with dynamic pressure for fourth-order control law. R_u = 0.00001.

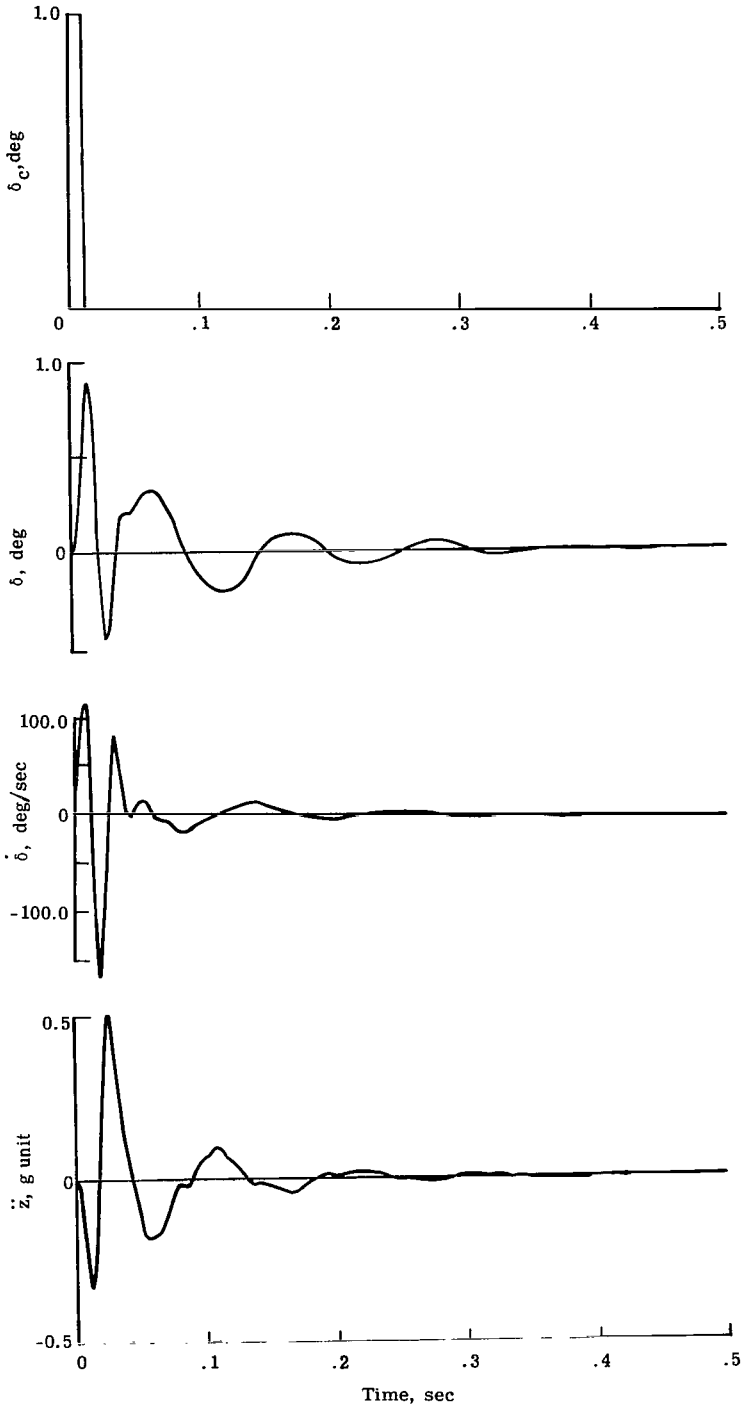

(a) Full-order control law.

Figure 13.- Transient response due to pulse control input with full-order and fourth-order control laws. q = 7.66 kPa.

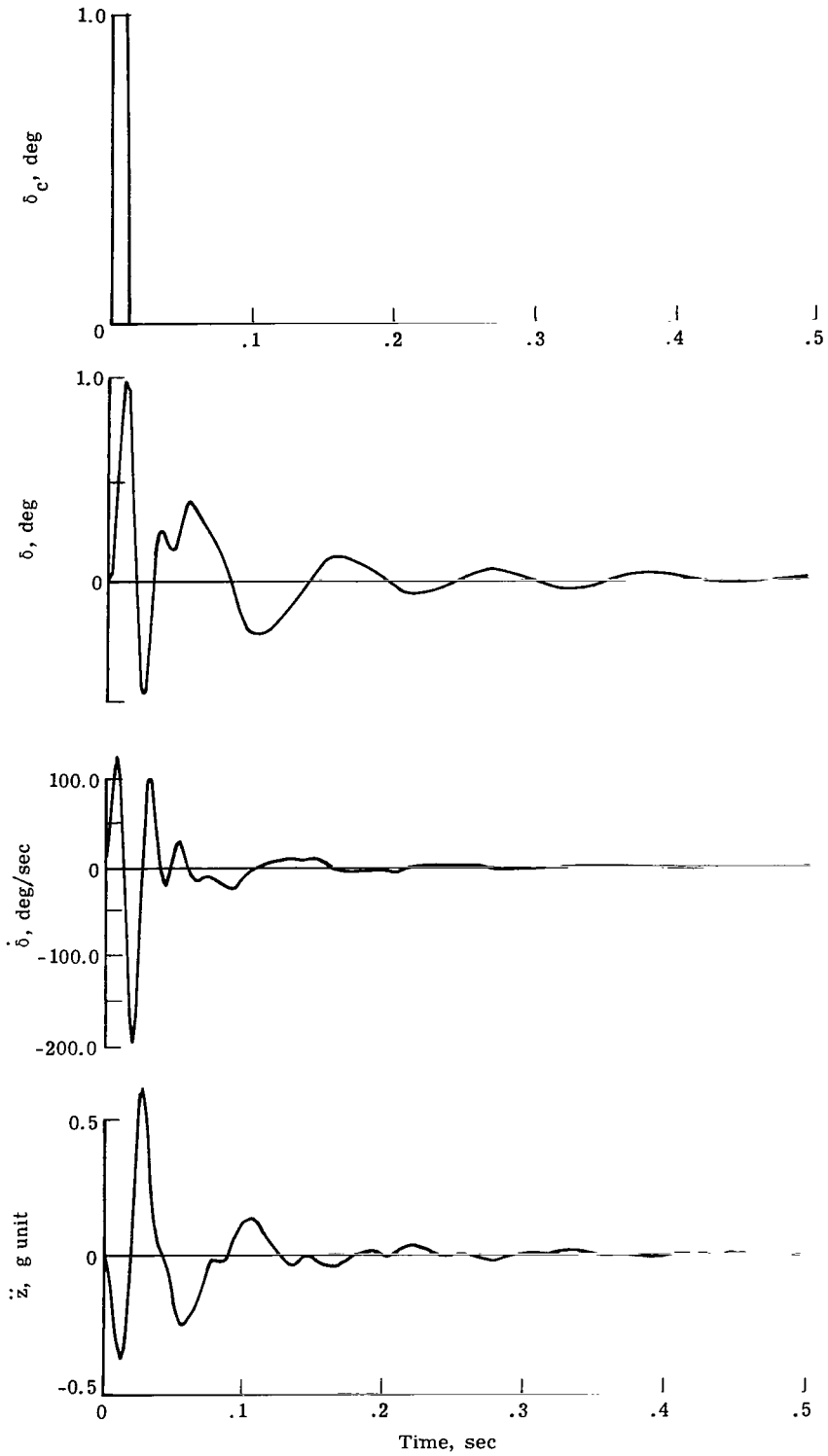

(b) Fourth-order control law.

Figure 13.- Concluded.

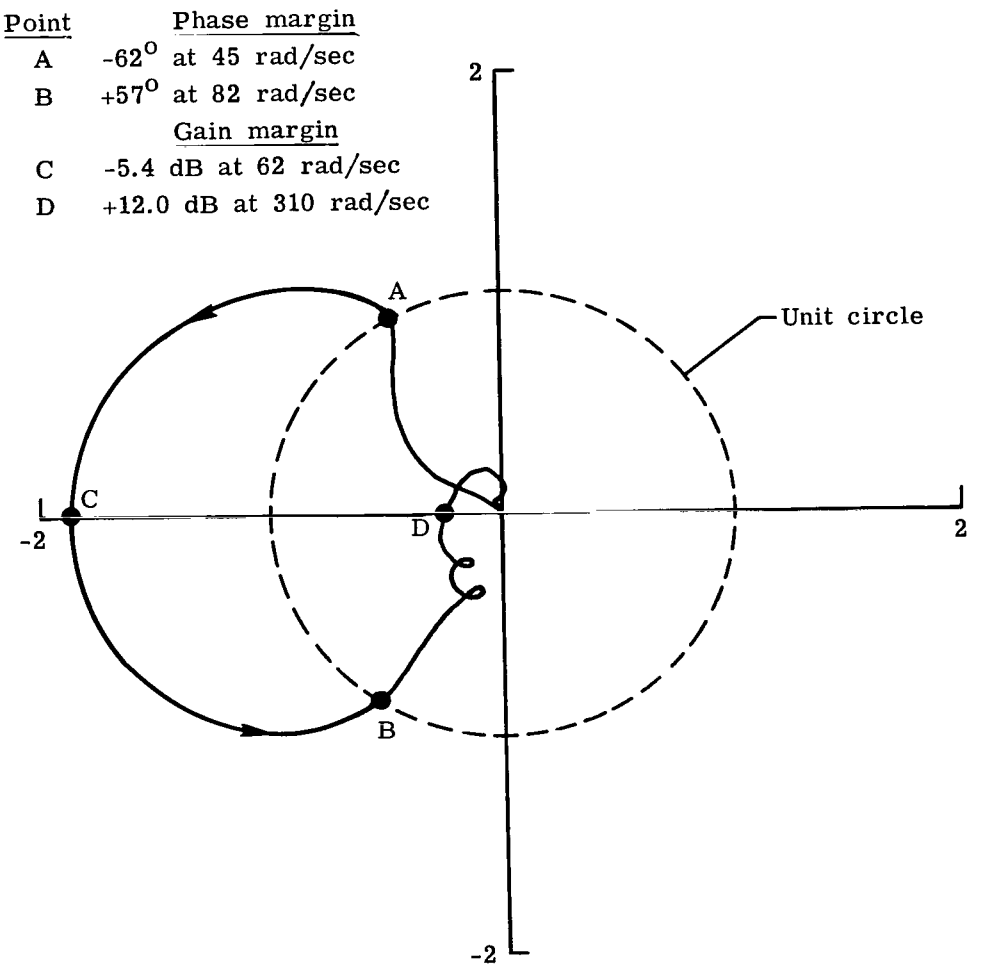

Figure 14.- Nyquist diagram of 65th-order plant model plus 4th-order control law (designed with 25th-order plant model). q = 7.66 kPa (arrows indicate increasing frequency). R_u = 0.00001.

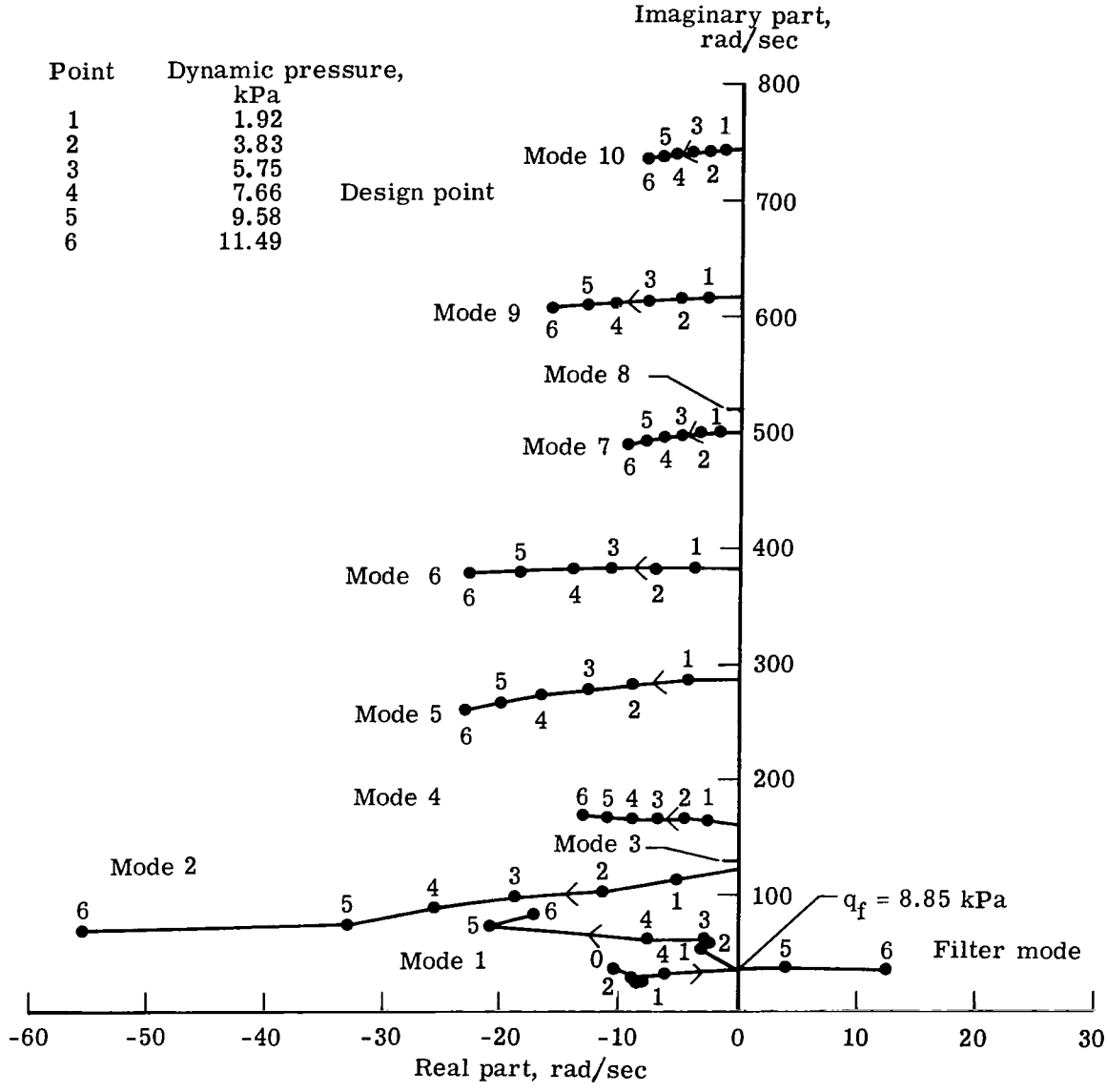

Figure 15.- Closed-loop dynamic-pressure root locus of 65th-order plant plus 4th-order control law (designed with 25th-order plant). R_u = 0.00001.

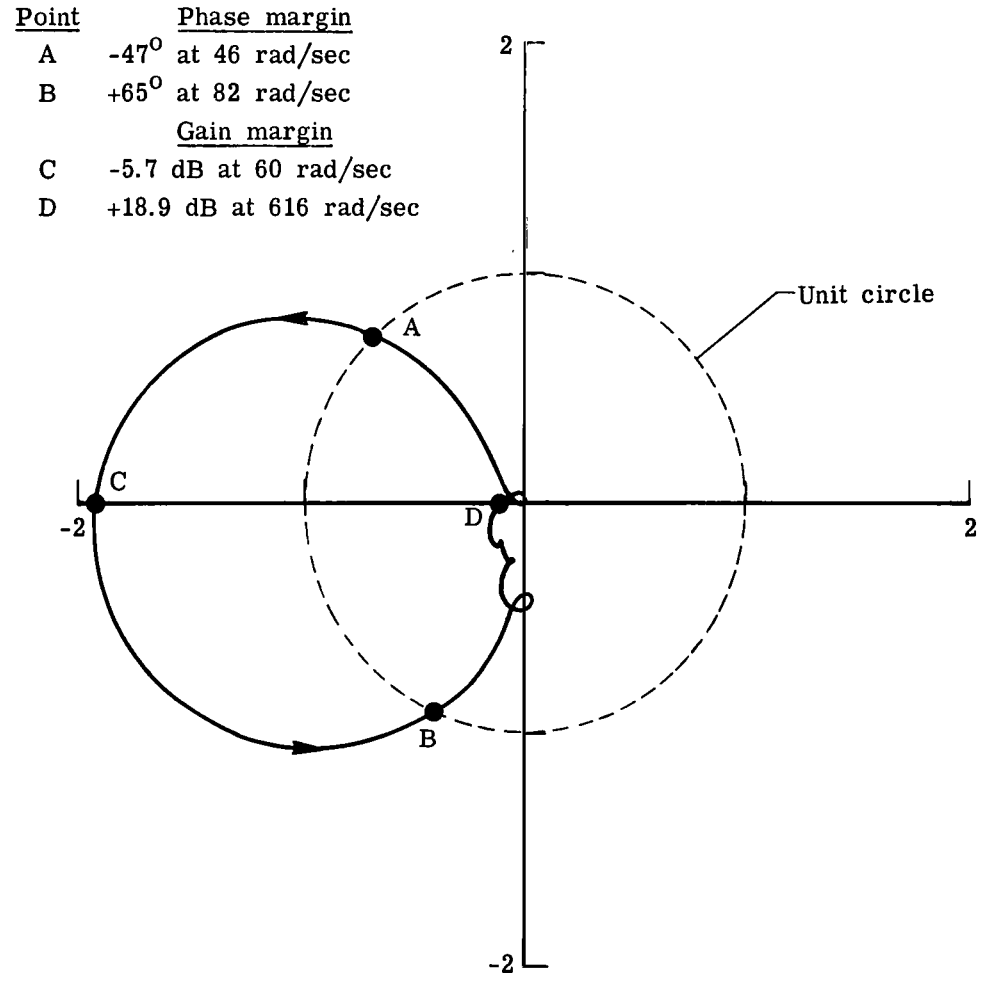

(a) Full order.

Figure 16.- Nyquist diagram of plant plus full-order control law and 4th-order control law designed by various methods for 25th-order plant. q = 7.66 kPa.

Point	Phase margin
A	-17^{o} at 38 rad/sec
B	$+57^{o}$ at 129 rad/sec
	Gain margin
C	-10.3 dB at 59 rad/sec
D	+6.5 dB at 254 rad/sec

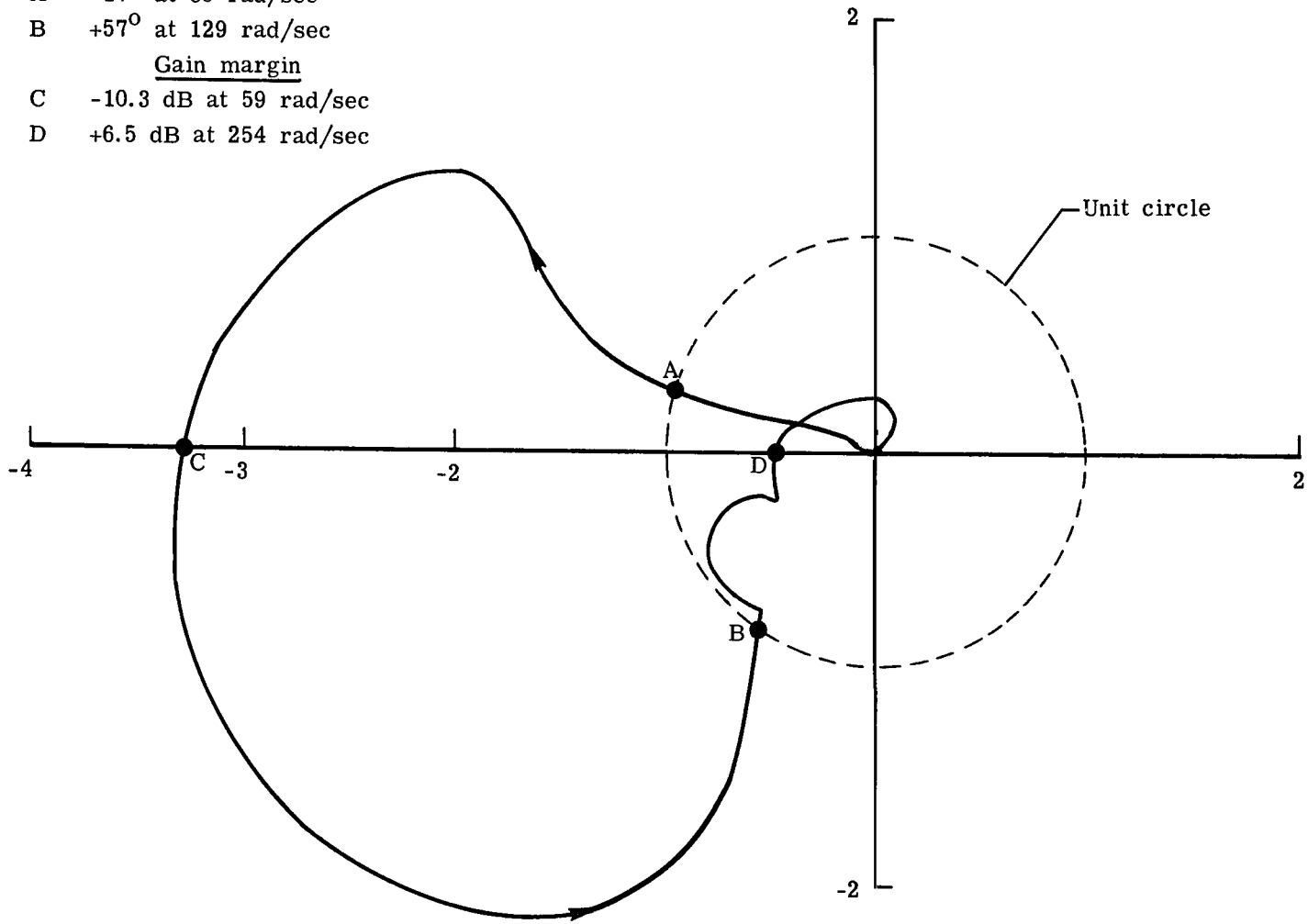

(b) Truncation method.

Figure 16.- Continued.

Point	Phase margin
A	-55^{o} at 46 rad/sec
B	$+38^{o}$ at 97 rad/sec
	Gain margin
C	-7.1 dB at 62 rad/sec
D	+6.0 dB at 164 rad/sec

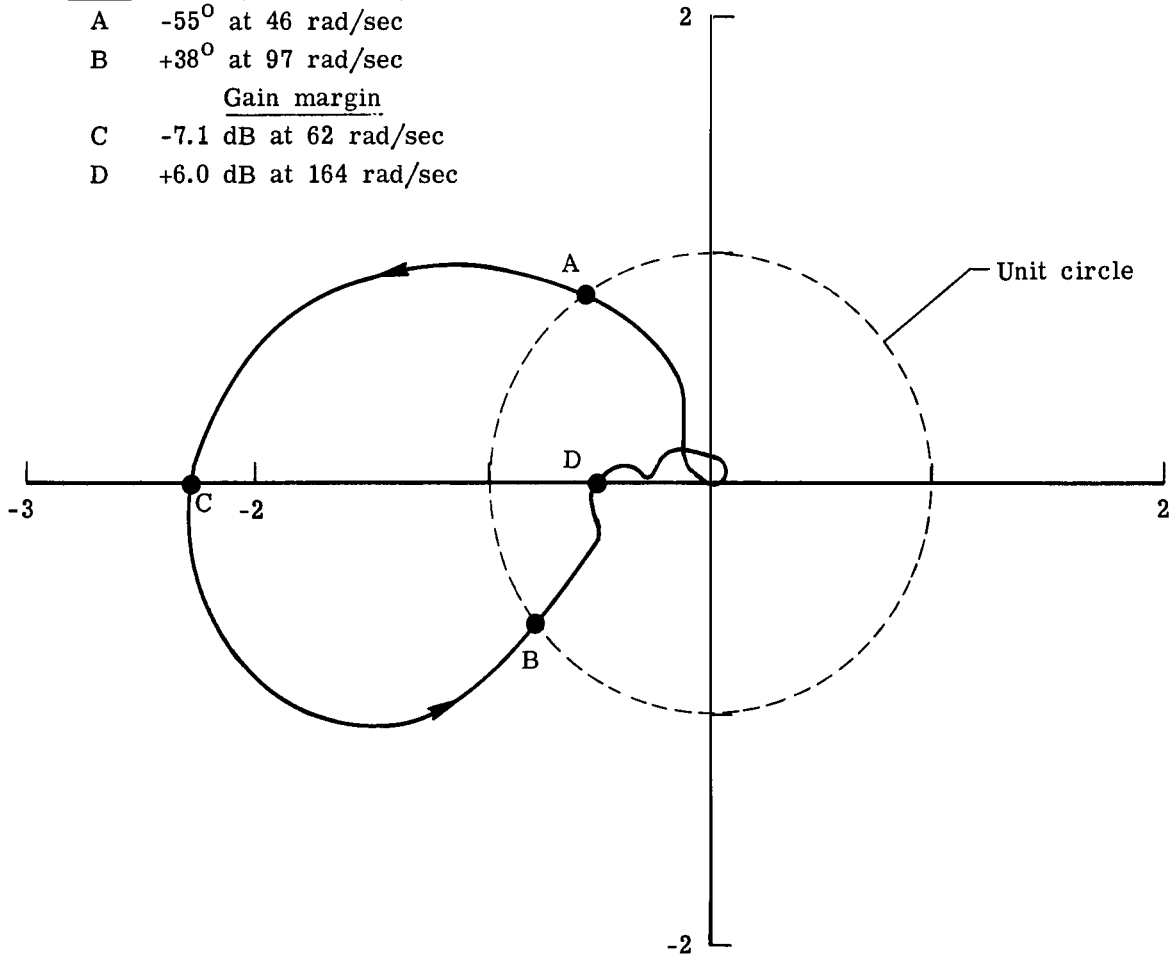

(c) Residualization method.

Figure 16.- Continued.

Point	Phase margin
A	-46^{o} at 47 rad/sec
B	$+53^{o}$ at 83 rad/sec
	Gain margin
C	-5.0 dB at 60 rad/sec
D	+12.3 dB at 314 rad/sec

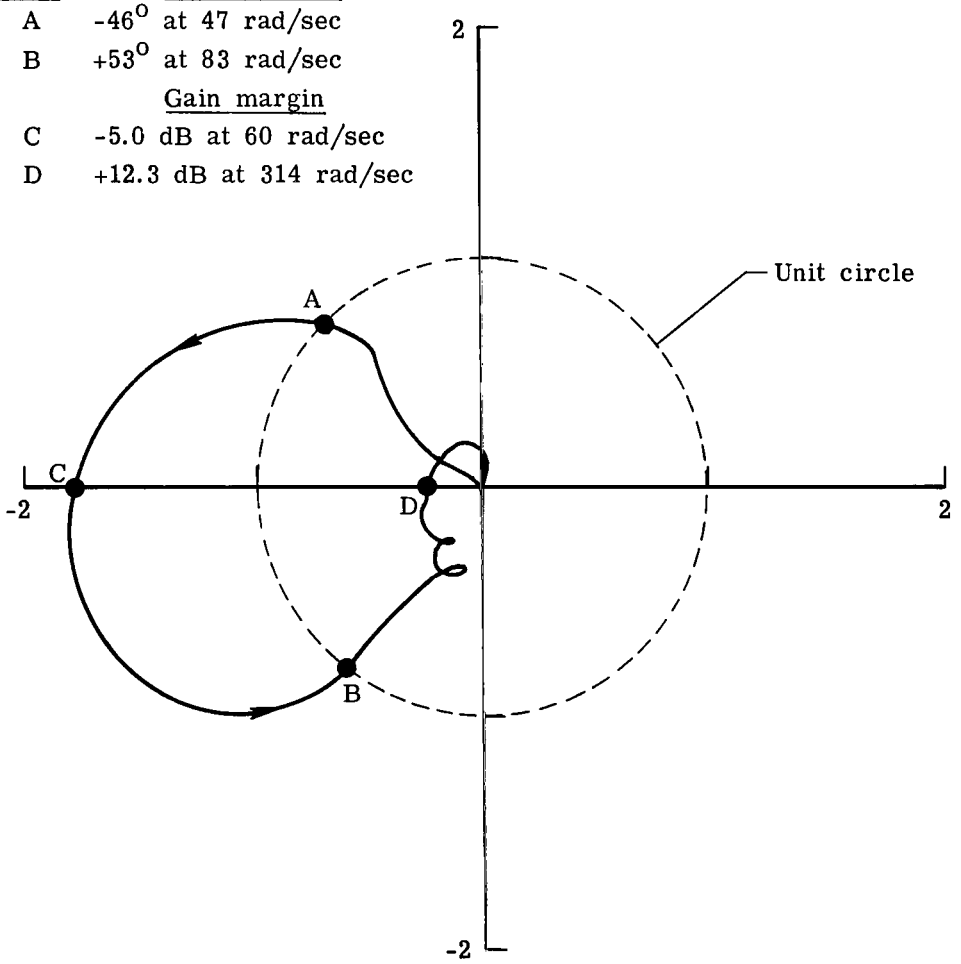

(d) Reoptimization (present) method.

Figure 16.- Concluded.

1. Report No.	2. Government Accession No.	3. Recipient's Catalog No.
NASA TP-1876		

4. Title and Subtitle
A METHOD FOR OBTAINING REDUCED-ORDER CONTROL LAWS FOR HIGH-ORDER SYSTEMS USING OPTIMIZATION TECHNIQUES

5. Report Date
August 1981

6. Performing Organization Code
505-33-63-02

7. Author(s)
Vivek Mukhopadhyay, Jerry R. Newsom, and Irving Abel

8. Performing Organization Report No.
L-14355

9. Performing Organization Name and Address
NASA Langley Research Center
Hampton, VA 23665

10. Work Unit No.

11. Contract or Grant No.

12. Sponsoring Agency Name and Address
National Aeronautics and Space Administration
Washington, DC 20546

13. Type of Report and Period Covered
Technical Paper

14. Sponsoring Agency Code

15. Supplementary Notes
Vivek Mukhopadhyay: NRC-NASA resident research associate.
Jerry R. Newsom and Irving Abel: Langley Research Center.

16. Abstract

A method of synthesizing reduced-order optimal feedback control laws for a high-order system is developed. A nonlinear programing algorithm is employed to search for the control law design variables that minimize a performance index defined by a weighted sum of mean-square steady-state responses and control inputs. An analogy with the linear quadratic Gaussian (LQG) solution is utilized to select a set of design variables and their initial values. To improve the stability margins of the system, an input-noise adjustment procedure is used in the design algorithm. The method is applied to the synthesis of an active flutter-suppression control law for a wind-tunnel model of an aeroelastic wing. The reduced-order controller is compared with the corresponding full-order controller and found to provide nearly optimal performance. The performance of the present method appeared to be superior to that of two other control law order-reduction methods. The study indicates that by using the present algorithm, nearly optimal low-order control laws with good stability margins can be synthesized.

17. Key Words (Suggested by Author(s))
Active controls
Optimization
Reduced-order controllers

18. Distribution Statement
Unclassified - Unlimited

Subject Category 63

19. Security Classif. (of this report)	20. Security Classif. (of this page)	21. No. of Pages	22. Price
Unclassified	Unclassified	65	A04

For sale by the National Technical Information Service, Springfield, Virginia 22161

NASA-Langley, 1981

2 1 1U,G, 081881 S00903DS
DEPT OF THE AIR FORCE
AF WEAPONS LABORATORY
ATTN: TECHNICAL LIBRARY (SUL)
KIRTLAND AFB NM 87117